Magyarhoni Földtani Társulat
Földtani Közlöny
Hungarian Geological Society

154/3, 329–346., Budapest, 2024

DOI: 10.23928/foldt.kozl.2024.154.3.329

Cluster analysis on a suite of upper mantle xenoliths from the Nógrád–Gömör Volcanic Field (Northern Pannonian Basin)

Patkó, Levente[1,2]*, Kuslits, Lukács[1], Czirok, Lili[3], Liptai, Nóra[2]

[1]HUN-REN Institute of Earth Physics and Space Science, Sopron, Hungary
[2]MTA FI Lendület Pannon LitH_2Oscope Research Group, HUN-REN Institute of Earth Physics and Space Science, Sopron, Hungary
[3]Quantectum Earthquake Forecasting Center, Ljubljana, Slovenia
*corresponding author: patko.levente@epss.hun-ren.hu

Klaszteranalízis a Nógrád–Gömör Vulkáni Területről (észak Pannon-medence) származó felsőköpeny xenolit sorozaton

Összefoglalás

A Nógrád–Gömör Vulkáni Terület feltehetően a legalaposabban kutatott felsőköpeny xenolit lelőhely a Kárpát–Pannon régióban. A kutatók a begyűjtött felsőköpeny xenolitok tucatjait számos nézőpont alapján vizsgálták az elmúlt évtizedekben. Jelen tanulmányhoz kapcsolódóan a területről elérhető tudományos közleményeket áttekintettük, és a bennük közölt, xenolitokra vonatkozó főelemgeokémiai adatokat kigyűjtöttük egy adatbázis felépítésének a céljából. A létrehozott adatbázis 112 xenolit kőzetalkotó ásványainak a geokémiai adatait tartalmazza. Ezt követően az összegyűjtött adatokon klaszteranalízist hajtottunk végre a CluStress algoritmus alkalmazásával, amely 2 főcsoport (I és II) és azokon belül további 17 csoport elkülönítését eredményezte. Az I-es főcsoport két alegységre osztható I/a és I/b főcsoportok). Az I/a főcsoporthoz tartozó xenolitok nagy ortopiroxén/klinopiroxén ásványos összetétel aránnyal (többnyire >1,5) és olivin Mg-számokkal (uralkodóan >0,89) jellemezhetők. Ezzel szemben az I/b főcsoportba sorolt xenolitok kis ortopiroxén/klinopiroxén ásványos összetétel hányadossal (többnyire <1) és olivin Mg-számokkal (uralkodóan <0,89) bírnak. A legtöbb xenolit (a besorolt xenolitok ~50%-a) az I/a főcsoporton belüli 1-es csoportba került, amely Nógrád–Gömör majdnem minden xenolit lelőhelyén előfordul. Az 1-es csoport xenolitjai a főelem-geokémiájuk vonatkozásában szűk tartományban változnak. Ezeket a kőzeteket az előfordulási gyakoriságuk és térbeli elterjedésük okán a terület alatti átlagos (háttér) litoszferikus köpenyként azonosítottuk. A többi csoport fejlődéstörténetét geokémiai tulajdonságaiknak köszönhetően többnyire képesek voltunk meghatározni. A megkülönböztetett 17 csoporton belül legalább 11 csoport xenolitjai esetén (a besorolt xenolitok ~35%-a) feltételezhető, hogy kialakulásuk szorosan kapcsolódik a neogén alkáli bazaltos vulkanizmushoz. Ez azt sugallja, hogy a Kárpát–Pannon régió vulkáni területeinek preneogén gyökérzónája jelentősen átalakulhatott a felfelé mozgó bazaltos olvadékok és a falkőzet intenzív kölcsönhatásának az eredményeként az utóbbi ~10 millió évben.

Tárgyszavak: Nógrád–Gömör Vulkáni Terület, felsőköpeny xenolitok, főelem-geokémia, klaszteranalízis

Abstract

The Nógrád–Gömör Volcanic Field is one of the most thoroughly studied upper mantle xenolith-bearing localities in the Carpathian–Pannonian region. Dozens of upper mantle xenoliths collected there have been investigated from various aspects in the past decades. Major element compositions of upper mantle xenoliths available in scientific papers on the Nógrád–Gömör xenoliths were extracted to build a database. This database includes the geochemical composition of the rock-forming minerals (olivine, pyroxenes, spinel) of 112 upper mantle xenoliths. Using the data compiled in this database, we applied the CluStress algorithm to perform cluster analysis. The results led to the division of 2 supergroups (I and II) and 17 groups within them. Supergroup I was split into two subgroups (Supergroup I/a and I/b). The xenoliths of Supergroup I/a and I/b are distinguished by their orthopyroxene/clinopyroxene modal composition ratios (mainly >1.5 and <1, respectively) as well as their olivine Mg-numbers (dominantly >0.89 and <0.89, respectively). Most of the xenoliths (~50% of all classified xenoliths) were sorted into Group 1 within Supergroup I/a, and they appear at almost all xenolith-bearing localities in the Nógrád–Gömör. The Group 1 xenoliths exhibit narrow compositional ranges regarding their major element relationships. Due to their common occurence and spatial distribution, these rocks were considered to represent an ambient lithospheric mantle underneath the study area. The geochemical characteristics of the other groups allowed their linking to different events described in former scientific works. At least 11 out of the 17 distinguished groups (i.e. ~35% of the classified xenoliths) are strongly related to the Neogene alkali basaltic volcanism. This suggests that the pre-Neogene rootzones of volcanic fields in the Carpathian–Pannonian region were significantly modified by intensive melt-rock reactions between upward migrating basaltic melts and wall rocks, which took place in the last ~10 million years.

Keywords: Nógrád–Gömör Volcanic Field, upper mantle xenoliths, major element geochemistry, cluster analysis

Introduction

In science, similar to other areas of life, increasing amounts of data are being accumulated. Geology is no exception, although gathering data is often challenging (e.g., requires time-consuming field or lab work). The wide application of analytical techniques led to a compilation of geological databases consisting of rock and mineral compositions [PetDB (http://www.earthchem.org/petdb) and GEOROC (http://georoc.mpch-mainz.gwdg.de/georoc/)], geochronological data [Geochron (https://www.geochron.org/)], paleomagnetic and partition coefficient values [Earth Reference Data and Models (https://earthref.org/)], spectral characteristics of nominally anhydrous minerals [PULI (http://puli.mfgi.hu/)], etc. Such compilations help with finding relevant references comparable to our results and making regional to global inferences. Despite their easy accessibility, databases are hard to overview and relationships, which are too complex to be extracted by descriptive statistics, may remain hidden.

In this situation, machine learning (ML), a branch of artificial intelligence, can help as it is capable of exploiting information stored in large datasets. ML is a set of algorithms and techniques that can automatically explore relations in the data to make predictions or decisions (MURPHY 2012). The major application fields of machine learning are classification, clustering, regression, dimensionality reduction and preprocessing (PEDREGOSA et al. 2011). Clustering is an unsupervised ML method aimed at grouping similar instances into sets known as clusters. In various branches of geology, such as geochemistry (DAWSON & STEPHENS 1975), volcanology (CORTÉS et al. 2007, GLEESON et al. 2021, BOSCHETTY et al. 2022, HENCZ et al. 2023), sedimentology (BOROVEC 1996, KALKREUTH et al. 2010, KIM et al. 2013), mineralogy (JERRAM & CHEADLE 2000, LACH-HAB et al. 2010) and exploration geology (JANSSON et al. 2022, GONÇALVES et al. 2024, SADEGHI et al. 2024), the use of various clustering methods is prevalent. These prior examples demonstrate that although geological databases are often limited in size, clustering is a useful tool to answer questions in the diverse field of geology.

Hundreds of upper mantle xenoliths hosted by widespread Neogene alkali basalts in the Carpathian–Pannonian region (CPR) (*Figure 1, a*) have been intensively studied in the last decades (EMBEY-ISZTIN et al. 1989, BALI et al. 2007, FALUS et al. 2008, HIDAS et al. 2010, BERKESI et al. 2012, ARADI et al. 2017). Most of these studies include detailed major and trace element analyses of the rock-forming minerals such as olivine, orthopyroxene, clinopyroxene and spinel. Additionally, data are also available on accessory phases including amphibole, apatite, ilmenite, zircon and rutile (ZANETTI et al. 1995, VASELLI et al. 1995, COLTORTI et al. 2007, BALI et al. 2018, LANGE et al. 2023). Therefore, a robust geochemical knowledge of upper mantle xenoliths is available in the literature, scattered in many publications. Probably the most investigated locality among the xenolith-bearing Neogene basalts in the CPR is the Nógrád–Gömör Volcanic Field (NGVF) (*Figure 1, b*). In the NGVF, the number of both the studied xenoliths and the applied technics is large, including various geochemical (HOVORKA & FEJDI 1980, SZABÓ & TAYLOR 1994, SZABÓ & BODNAR 1995, SZABÓ et al. 1996, KONEČNÝ et al. 1999, LIPTAI et al. 2017, PATKÓ et al. 2020) and geophysical approaches (KLÉBESZ et al. 2015, LIPTAI et al. 2019, PATKÓ et al. 2021a).

This study focuses on 112 upper mantle xenoliths (with 114 lithologies due to composite xenoliths) collected in the NGVF. Our principal goals were to 1) build a uniform geochemical database including the major element compositions of the rock-forming minerals based on former publications, and 2) implement cluster analysis on the assembled database in order to reveal the geochemically, and thus likely genetically different mantle volumes underneath the study area.

Geological background

The Pannonian Basin is situated in Central Europe surrounded by the Alpine, Carpathian and Dinaric orogenic belts (*Figure 1, a*). Understanding the complex tectonic evolution of this extensional back-arc basin has been the focus of many studies (ROYDEN et al. 1982, FODOR et al. 1999, HORVÁTH et al. 2006, KOVÁCS et al. 2012, BALÁZS et al. 2016). The Pannonian Basin consists of two tectonic mega-units with different affinities, referred to as ALCAPA in the northwest and Tisza–Dacia in the southeast (CSONTOS & VÖRÖS 2004), divided by the Mid-Hungarian shear zone (CSONTOS & NAGYMAROSY 1998) (*Figure 1, a*). The juxtaposition of the

→ **Figure 1.** (a) Simplified geological map of the Carpathian–Pannonian region (after CSONTOS & VÖRÖS 2004) with the assumed ALCAPA – Tisza–Dacia microplate boundary (after CSONTOS & NAGYMAROSY 1998). Xenolith-bearing Neogene alkali basalt localities (SZABÓ et al. 2004) are depicted using abbreviations: SBVF: Styrian Basin Volcanic Field; LHPVF: Little Hungarian Plain Volcanic Field; BBHVF: Bakony–Balaton Highland Volcanic Field; NGVF: Nógrád–Gömör Volcanic Field; PMVF: Perşani Mountains Volcanic Field. (b) Alkali basalt outcrops and xenolith sampling locations in the Nógrád–Gömör Volcanic Field (modified after JUGOVICS 1971); quarries or outcrops from NW to SE can be divided into three parts as follows: northern segment: Podrečany [Patakalja] (NPY), Mašková [Maskófalva] (NMS), Jelšovec [Jelsőc] (NJS); central segment: Fil'akovo-Kerčik [Fülek–Kercsik-tető] (NFL), Trebel'ovce [Terbeléd] (NTB), Fil'akovské Kováče [Fülekkovácsi] (NFK), Ratka [Rátka] (NFR), Mačacia [Macskakő] (NMC), Magyarbánya (NMM), Eresztvény (NME), Nagy-Salgó (NNS) and southern segment: Bárna-Nagykő (NBN), Bárna-Kiskő (NBK)

→ ***1. ábra*** *(a) A Kárpát–Pannon régió egyszerűsített földtani térképe (CSONTOS & VÖRÖS 2004 alapján) az ALCAPA és a Tisza–Dácia mikrolemezek feltételezett határával (CSONTOS & NAGYMAROSY 1998 alapján). A neogén korú, xenolitot tartalmazó alkáli bazaltos lelőhelyek (SZABÓ et al. 2004) a következő rövidítésekkel bírnak: SBVF: Stájer-medence Vulkáni Terület, LHPVF: Kisalföld Vulkáni Terület, BBHVF: Bakony–Balaton-felvidék Vulkáni Terület, NGVF: Nógrád–Gömör Vulkáni Terület, PMVF: Persány-hegység Vulkáni Terület. (b) Alkáli bazalt előfordulások és xenolit lelőhelyek a Nógrád–Gömör Vulkáni Területen (JUGOVICS 1971 után módosítva). A kőfejtők és feltárások ÉNy-ról DK felé három szegmensre oszthatók. Ezek név szerint a következők: északi szegmens: Podrečany [Patakalja] (NPY), Mašková [Maskófalva] (NMS), Jelšovec [Jelsőc] (NJS); központi szegmens: Fil'akovo-Kerčik [Fülek–Kercsik-tető] (NFL), Trebel'ovce [Terbeléd] (NTB), Fil'akovské Kováče [Fülekkovácsi] (NFK), Ratka [Rátka] (NFR), Mačacia [Macskakő] (NMC), Magyarbánya (NMM), Eresztvény (NME), Nagy-Salgó (NNS) és déli szegmens: Bárna-Nagykő (NBN), Bárna-Kiskő (NBK)*

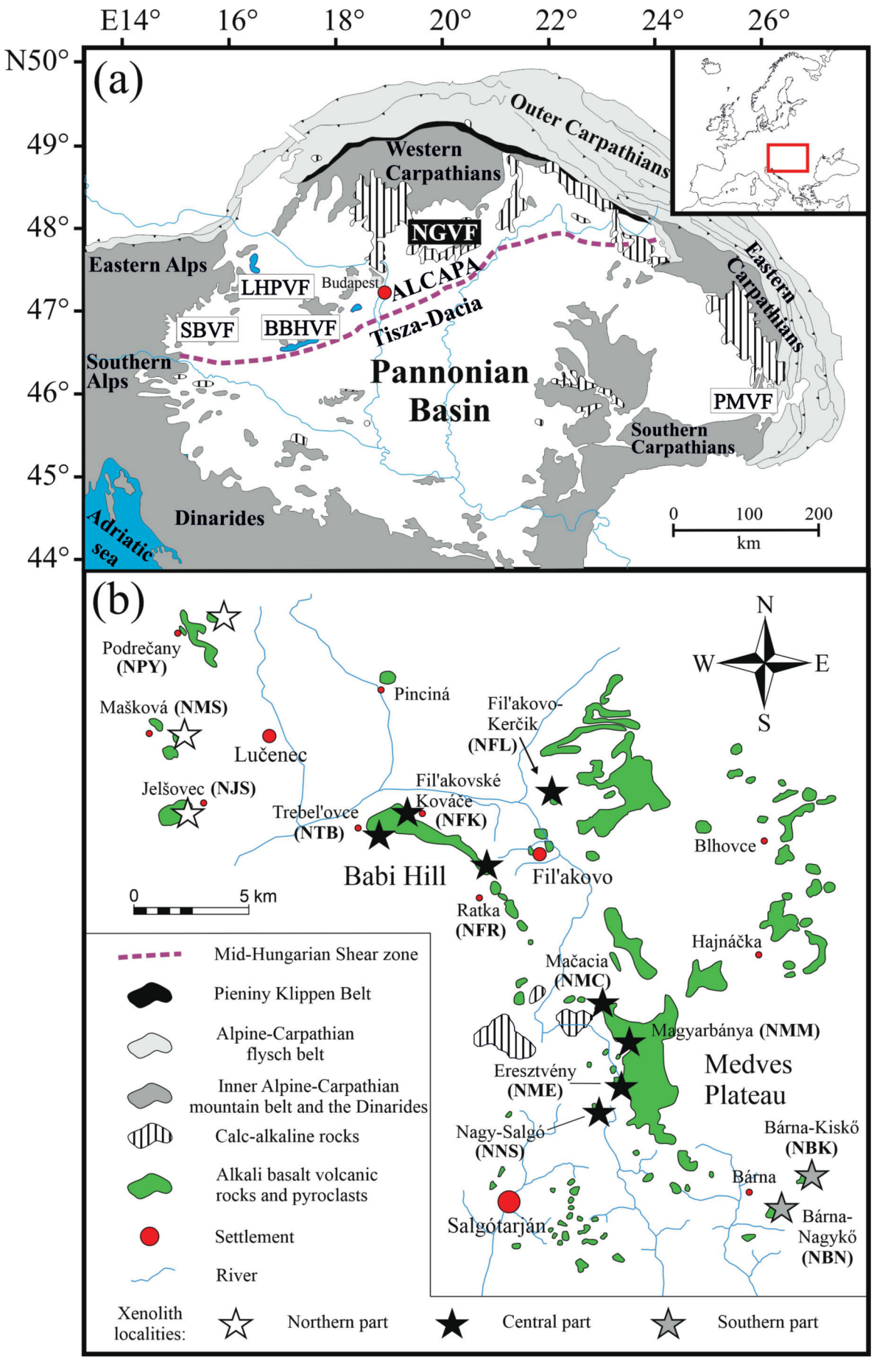
E14°
16°
18°
20°
22°
24°
26°
N50°
49°
48°
47°
46°
45°
44°
(a)
Outer Carpathians
Western Carpathians
NGVF
Eastern Alps
LHPVF
Budapest
ALCAPA
Tisza-Dacia
Eastern Carpathians
SBVF
BBHVF
Southern Alps
Pannonian Basin
PMVF
Southern Carpathians
Dinarides
Adriatic sea
0 100 200
km
(b)
N
W
E
S
Podrečany (NPY)
Pinciná
Mašková (NMS)
Fil'akovo-Kerčik (NFL)
Lučenec
Jelšovec (NJS)
Fil'akovské Kováče (NFK)
Trebel'ovce (NTB)
Blhovce
Babi Hill
Fil'akovo
0 5 km
Ratka (NFR)
Hajnáčka
Mačacia (NMC)
Magyarbánya (NMM)
Medves Plateau
Eresztvény (NME)
Nagy-Salgó (NNS)
Bárna-Kiskő (NBK)
Bárna
Salgótarján
Bárna-Nagykő (NBN)
Mid-Hungarian Shear zone
Pieniny Klippen Belt
Alpine-Carpathian flysch belt
Inner Alpine-Carpathian mountain belt and the Dinarides
Calc-alkaline rocks
Alkali basalt volcanic rocks and pyroclasts
Settlement
River
Xenolith localities:
Northern part
Central part
Southern part

mega-units occurred during the latest Oligocene to early Miocene after the extrusion of the ALCAPA mega-unit (KÁZMÉR & KOVÁCS 1985) due to the northward movement of the Adriatic microplate and slab rollback (FODOR et al. 1999). Significant extension took place in the Pannonian Basin during the Neogene (HORVÁTH et al. 2006) leading to considerable thinning of the lithosphere and asthenosphere doming (HORVÁTH 1993, HUISMANS et al. 2001, KALMÁR et al. 2023, RUBÓCZKI et al. 2024). Finally, the collision of the mega-units (ALCAPA and Tisza–Dacia) with the stable European platform led to a compressive tectonic regime from the late Miocene (HORVÁTH & CLOETINGH 1996, BADA et al. 2007).

All stages of the basin evolution were accompanied by widespread volcanism in the Carpathian–Pannonian region (CPR) characterized by silicic, calc-alkaline and alkali volcanic products (SZABÓ et al. 1992, SEGHEDI & DOWNES 2011). In the study area, both garnet-bearing calc-alkaline (HARANGI et al. 2001) and alkali volcanic rocks (KONEČNÝ V. et al. 1995) occur (*Figure 1, b*). The formation of monogenetic alkali basalts, such as the ones comprising the study area of the NGVF (*Figure 1, b*), can be explained by adiabatic decompression melting of the asthenosphere related to an extension-associated upwelling (~20–8 Ma) (EMBEY-ISZTIN et al. 1993, HARANGI et al. 2015). Since decompression melting raises temporal controversies, it has recently been proposed that compression in the tectonic inversion stage of the CPR evolution may have squeezed partial melts out from the asthenosphere (KOVÁCS et al. 2020). The volcanic activity in the NGVF took place between 6.17 Ma and 1.35 Ma based on K–Ar dating (BALOGH et al. 1981). New results of combined U/Pb and (U–Th)/He geochronometry (HURAI et al. 2013) propose a slightly extended period for the volcanism (7–0.3 Ma).

The NGVF basalts host numerous crustal (KOVÁCS & SZABÓ 2005; HURAIOVÁ et al. 2005, 2017) and ultramafic xenoliths. Among the ultramafic xenoliths, based on the classification of FREY & PRINZ (1978), both Type-I (EMBEY-ISZTIN 1978, HOVORKA & FEJDI 1980, SZABÓ & TAYLOR 1994, KONEČNÝ et al. 1999, LIPTAI et al. 2017) and Type-II rocks (i.e., cumulates) (HURAIOVÁ et al. 1996, KOVÁCS et al. 2004, ZAJACZ et al. 2007) have been reported, representing volumes of the heterogeneous lithospheric mantle and underplated crystallized products in the vicinity of the Moho, respectively. The geochemical characteristics of Type-I xenoliths reveal that melt extraction (e.g. light rare earth element – LREE – depletion) and metasomatism (e.g. LREE enrichment) both occurred underneath the NGVF (LIPTAI et al. 2017). The enrichment can be linked to migrating silicate melts (SZABÓ et al. 1996, ZAJACZ et al. 2007, LIPTAI et al. 2021), sulfide melts (SZABÓ & BODNAR 1995, ZAJACZ & SZABÓ 2003, PATKÓ et al. 2021b) and fluids (HURAIOVÁ & KONEČNÝ 1994; SZABÓ & BODNAR 1996, 1998). The metasomatic fingerprints are dominantly linked to a recent (last 7 Ma) magmatic event that produced the xenolith-bearing host basalts and their surface forms as well (PATKÓ et al. 2020). Note that the effect of subduction-related fluids has also been explored underneath the NGVF based on the presence of Nb-poor amphiboles (LIPTAI et al. 2017). LIPTAI et al. (2017) argued that this suprasubduction character is an inherited feature representing a tectonic situation that existed in the Alpine collision zone, far from the current location of the NGVF. It is the extrusion that moved suprasubduction mantle volumes to their current position (KOVÁCS & SZABÓ 2008).

Database

The cluster analysis in this study is based on the major element geochemistry of the rock-forming constituents of upper mantle xenoliths (*Supplementary Table I*). These minerals and major elements are as follows: SiO_2, FeO, MnO, MgO, CaO, NiO for olivine, SiO_2, TiO_2, Al_2O_3, Cr_2O_3, FeO, MnO, MgO, CaO, Na_2O for orthopyroxene, SiO_2, TiO_2, Al_2O_3, Cr_2O_3, FeO, MnO, MgO, CaO, Na_2O, for clinopyroxene and TiO_2, Al_2O_3, Cr_2O_3, FeO, MnO, MgO, NiO for spinel. This database contains standardized electron microprobe-based results published in the following papers: HOVORKA & FEJDI (1980) (4 xenoliths); SZABÓ & TAYLOR (1994) (22 xenoliths and 2 extra lithologies appearing as veins); KONEČNÝ P. et al. (1995) (4 xenoliths); KONEČNÝ et al. (1999) (5 xenoliths); KOVÁCS et al. (2004) (6 xenoliths); ARADI et al. (2013) (6 xenoliths); LIPTAI et al. (2017) (53 xenoliths); PATKÓ et al. (2020) (12 xenoliths). Altogether, geochemical data of 112 upper mantle xenoliths (114 different lithologies) were compiled.

Applied cluster analysis algorithm (CluStress)

In this study, a clustering algorithm, named CluStress (CZIROK & KUSLITS 2018, CZIROK et al. 2022) was applied (the latest version of CluStress is available here: https://pypi.org/project/clu-stress/). This algorithm does not require to set hyperparameters (e.g. number of clusters, number of elements within a cluster, etc.). However, there is one optional parameter that can be used for filtering outliers from the input database.

The algorithm utilizes the non-reflexivity of the nearest neighbor principle after calculating datapoint distances to reveal linkages. The linkage rule in CluStress is significantly simpler than in the methods of hierarchical clustering (CAMPELLO et al. 2013) or hierarchical density-based clustering applications with noise (HDBSCAN) (MCINNES et al. 2017) methods.

An important peculiarity of the CluStress algorithm is that it allows to find the clustered nearest neighbors of unclustered points instead of the other way around. Therefore, CluStress leads to the separation of larger and more compact clusters, and avoids their merging with adjacent point classes, which have their own internal compactness. Furthermore, anoptional parameter for outlier detection is also

available to filter isolated and 'confusing' points. In this study, the authors executed the Box-Cox transformation (Box & Cox 1964) to filter the outliers from the initial database. The operation of this outlier parameter in CluStress is similar to the epsilon (Eps) value of DBSCAN (Ester et al. 1996, Campello et al. 2013) or HDBSCAN (McInnes et al. 2017), i.e., it sets a threshold for the distance of neighboring points. In this study, we fixed this Eps value to 1.5 to extract inappropriate, isolated data from the input dataset. The large number of sets is essentially a consequence of the algorithmic logic because it separates several small groups that have their own "clusterized" cores, which is useful mainly because the larger sets then become more compact.

The applied Python code is available here: https://github.com/lukacskuslits/clu-stress/tree/nearest_neighbors/tests.

The results (*Figure 2, a*) were illustrated using Umap technique (McInnes et al. 2020) that reduces the high-dimensional data to two dimensions while reasonably preserving the original distance relations of the data points. To reveal how the major element composition of different rock-forming minerals influences the clustering, vectors were created in the field of the two major principal components (*Figure 2, b*) (Pedregosa et al. 2011). The results suggest a negative correlation for the xenoliths, especially when all supergroups are considered (*Figure 2, b*). The obtained xenolith distribution along with the vectors for different major elements suggests that the classification is dominantly based on the geochemistry of olivines (the different olivine major element vectors align with the direction described by the xenoliths) (*Figure 2, b*). In contrast, the composition of orthopyroxenes only weakly influences the classification (*Figure 2, b*). Among the elements, iron content might play a key role in the classification, as it is represented by vectors for several minerals (olivine, clinopyroxene, spinel) along the xenolith trend (*Figure 2, b*).

Results

One hundred nine out of the 112 upper mantle xenoliths (i.e., 111 out of the 114 lithologies due to composite (veined) samples) were classified into two supergroups (*Figure 2, a*). The other three xenoliths did not fit with any groups using CluStress, and thus were not further considered (*Supplementary Table I*). The supergroups were separated based on the high-dimensional dataset visualized in two-dimensions using the Umap technique (*Figure 2, a*). Xenoliths of Supergroup I and II are dominated by peridotites (>40 vol.% olivine content) and pyroxenites (<40 vol.% olivine content), respectively (*Figure 3*). Supergroup I was split into two subgroups (Supergroup I/a and I/b). The xenoliths of Supergroup I/a are mostly lherzolites by their modal composition, with orthopyroxene/clinopyroxene ratios mainly >1.5 (*Figure 3*; *Supplementary Table I*). In contrast, xenoliths classified into Supergroup I/b are characterized by wehrlite dominance, meaning low orthopyroxene/clinopyroxene modal

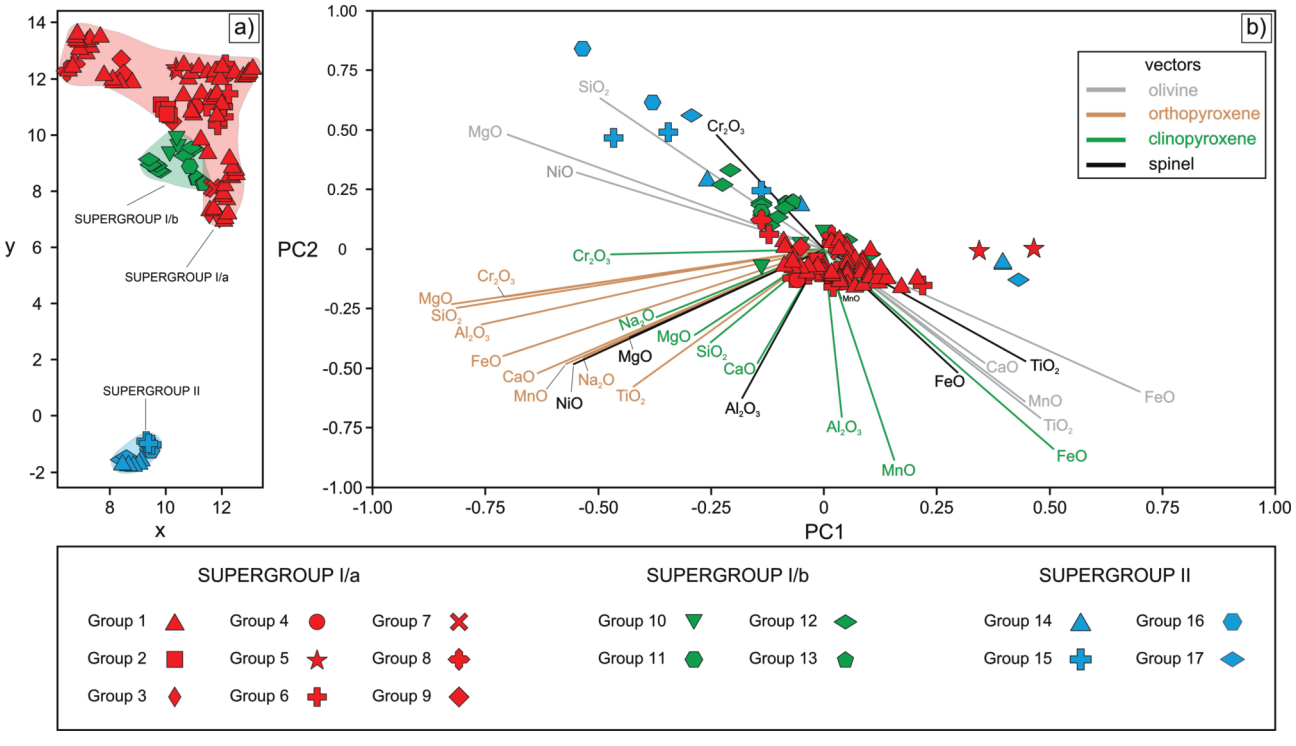

Figure 2. (a) The resulting clusters in the high-dimensional parameter space (defined by the major elements) projected into a two-dimensional (x-y) plane using the Umap technique (McInnes et al. 2020). (b) Xenolith data points in the field of the first two principal components (PC1 and PC2) (Pedregosa et al. 2011). Vectors show the contribution of different major element compositions

2. ábra. *(a) Sokdimenziós adatok kétdimenziós térbe (x-y mező) történő redukálása Umap algoritmus (McInnes et al. 2020) alkalmazásával. (b) Xenolit adatpontok a két főkomponens (PC1 és PC2) mezőjében (Pedregosa et al. 2011). A vektorok a különböző főelemek csoportosításra gyakorolt hatását hivatottak reprezentálni*

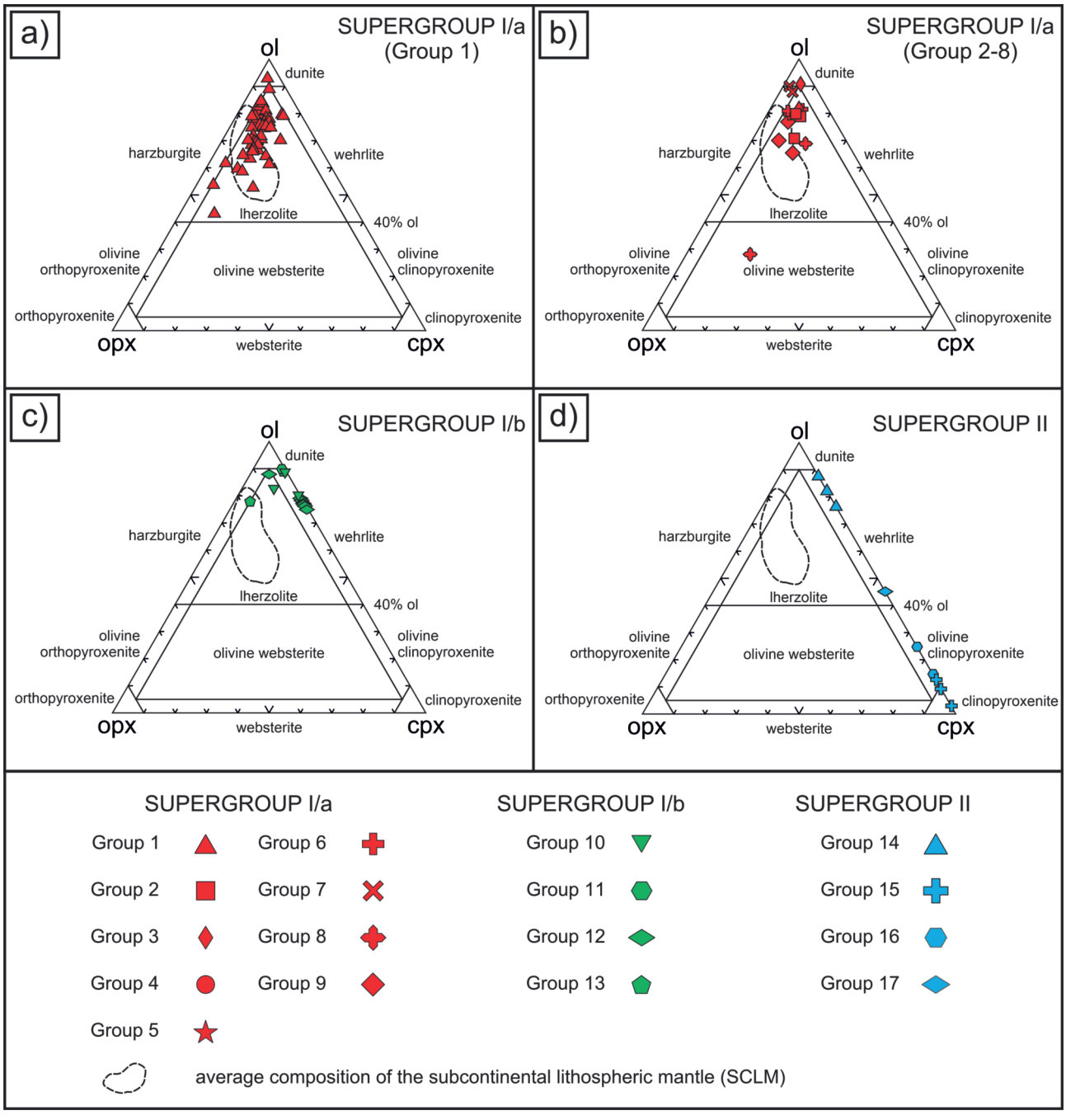

Figure 3. Modal composition of the (a) Group 1; (b) Group 2–13; (c) Group 15–17 and (d) Group 18–21 NGVF xenoliths on a STRECKEISEN (1976) diagram. The average composition of the European subcontinental lithospheric mantle (SCLM; DOWNES 1997) is indicated with a dashed line. Data of the NGVF xenoliths are taken from: HOVORKA & FEJDI (1980), SZABÓ & TAYLOR (1994), KOVÁCS et al. (2004), ARADI et al. (2013), LIPTAI et al. (2017), PATKÓ et al. (2020)

3. ábra. *A nógrád-gömöri xenolitok ásványos összetétele STRECKEISEN (1976) diagramon ábrázolva az (a) 1 csoport; (b) 2–13 csoportok; (c) 15–17 csoportok és (d) 18–21 csoportok vonatkozásában. Az ábrán az európai szubkontinentális litoszferikus köpeny (SCLM; DOWNES 1997) megjelenítése szaggatott vonallal történt. A nógrád-gömöri xenolitok adatainak forrása: HOVORKA & FEJDI (1980), SZABÓ & TAYLOR (1994), KOVÁCS et al. (2004), ARADI et al. (2013), LIPTAI et al. (2017), PATKÓ et al. (2020)*

→ **Figure 4.** Major element composition of the NGVF xenoliths. (a) Variation of Mg# vs. NiO in olivine; (b) variation of Mg# vs. MnO in orthopyroxene; (c) variation of Na_2O vs. Al_2O_3 in clinopyroxene; (d) variation of Mg# vs. SiO_2 in clinopyroxene; (e) variation of Mg# vs. TiO_2 in clinopyroxene; (f) variation of Al_2O_3–Cr_2O_3–TiO_2 x 100 in spinel. Data of the NGVF xenoliths are taken from: HOVORKA & FEJDI (1980), SZABÓ & TAYLOR (1994), KONEČNÝ P. et al. (1995), KONEČNÝ et al. (1999), KOVÁCS et al. (2004), ARADI et al. (2013), LIPTAI et al. (2017), PATKÓ et al. (2020)

→ ***4. ábra.*** *Nógrád-Gömör Vulkáni Terület xenolitjainak főelem-geokémiája. (a) Mg# és NiO összefüggése olivinben; (b) Mg# és MnO összefüggése ortopiroxénben; (c) Na_2O és Al_2O_3 összefüggése klinopiroxénben; (d) Mg# és SiO_2 összefüggése klinopiroxénben; (e) Mg# és TiO_2 összefüggése klinopiroxénben; (f) Al_2O_3-Cr_2O_3-TiO_2 x 100 összefüggése spinellben. A nógrád-gömöri xenolitok adatainak forrása: HOVORKA & FEJDI (1980), SZABÓ & TAYLOR (1994), KONEČNÝ P. et al. (1995), KONEČNÝ et al. (1999), KOVÁCS et al. (2004), ARADI et al. (2013), LIPTAI et al. (2017), PATKÓ et al. (2020)*

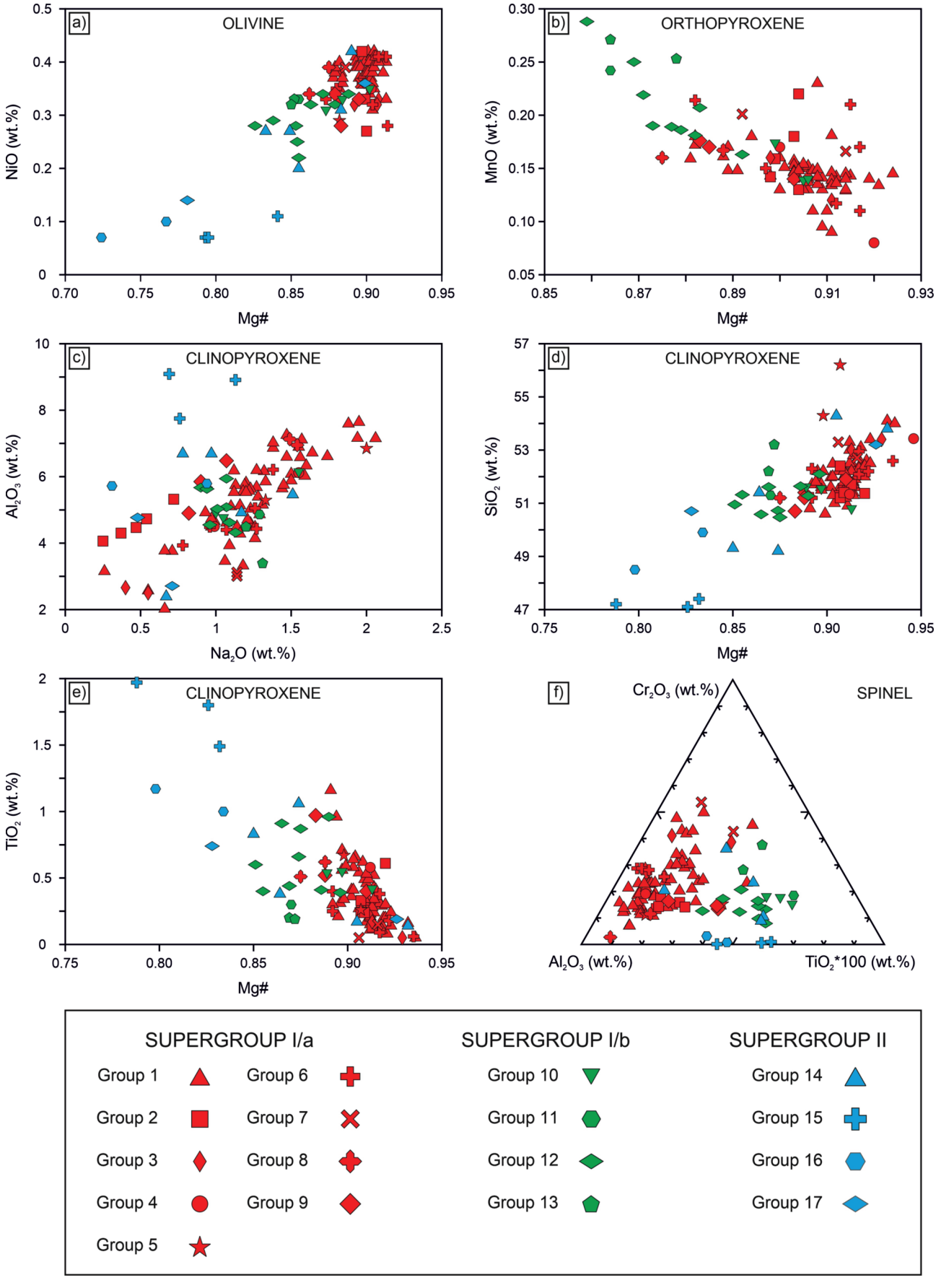
a)
OLIVINE
NiO (wt.%)
Mg#
b)
ORTHOPYROXENE
MnO (wt.%)
Mg#
c)
CLINOPYROXENE
Al2O3 (wt.%)
Na2O (wt.%)
d)
CLINOPYROXENE
SiO2 (wt.%)
Mg#
e)
CLINOPYROXENE
TiO2 (wt.%)
Mg#
f)
SPINEL
Cr2O3 (wt.%)
Al2O3 (wt.%)
TiO2*100 (wt.%)
SUPERGROUP I/a
Group 1
Group 2
Group 3
Group 4
Group 5
Group 6
Group 7
Group 8
Group 9
SUPERGROUP I/b
Group 10
Group 11
Group 12
Group 13
SUPERGROUP II
Group 14
Group 15
Group 16
Group 17

Table I. Modal and geochemical compositional ranges and average values (latter in brackets) of the supergroups defined by the applied cluster analyses
Abbreviations: ol – olivine; opx – orthopyroxene; cpx – clinopyroxene; sp – spinel

I. táblázat. *A klaszteranalízis által meghatározott szupercsoportok ásványos és kémiai összetételének tartományai és átlagértékei (utóbbi zárójelben)*
Rövidítések: ol – olivin; opx – ortopiroxén; cpx – klinopiroxén; sp – spinell

	Supergroup I/a				Supergroup I/b				Supergroup II			
	ol	opx	cpx	sp	ol	opx	cpx	sp	ol	opx	cpx	sp
modal composition	26-91 (72)	4-48 (16)	2-19 (9)	0-5 (2)	72-88 (79)	0.5-17 (3)	5-24 (15)	0.5-7 (2)	3-85 (38)	–	12-96 (52)	1-5 (2)
SiO_2	39.8-43.3 (40.8)	54.1-58.0 (55.5)	50.6-56.2 (52.1)	–	39.3-41.2 (40.1)	54.1-55.9 (55.2)	50.5-53.2 (51.6)	–	37.5-43.1 (39.8)	–	47.1-54.3 (50.5)	–
TiO_2	–	0.01-0.25 (0.08)	0.05-1.16 (0.35)	0.03-0.49 (0.14)	–	0.05-0.25 (0.10)	0.19-0.96 (0.48)	0.32-1.08 (0.61)	–	–	0.14-1.97 (0.86)	0.14-0.93 (0.56)
Al_2O_3	–	1.86-5.00 (3.73)	2.02-7.64 (5.26)	4.89-64.5 (47.8)	–	1.95-3.91 (2.86)	3.39-6.15 (4.88)	22.9-51.0 (36.9)	–	–	2.39-9.09 (5.88)	32.0-60.4 (50.3)
Cr_2O_3	–	0.08-0.67 (0.42)	0.18-1.41 (0.91)	1.98-46.4 (18.6)	–	0.30-0.56 (0.46)	0.77-1.36 (1.09)	10.9-39.9 (23.0)	–	–	0.07-1.01 (0.57)	0.14-33.9 (10.9)
FeO	8.37-13.1 (9.94)	5.31-8.05 (6.33)	1.64-3.86 (2.81)	9.96-20.3 (12.7)	9.78-16.6 (13.4)	6.23-9.21 (8.04)	2.67-4.86 (3.97)	13.3-24.0 (20.0)	8.88-25.2 (15.8)	–	2.27-6.51 (4.36)	11.2-24.6 (19.5)
MnO	0.04-0.24 (0.15)	0.08-0.23 (0.15)	0.04-0.13 (0.08)	0.07-0.55 (0.12)	0.15-0.28 (0.22)	0.14-0.29 (0.21)	0.08-0.17 (0.12)	0.13-0.31 (0.20)	0.15-0.38 (0.25)	–	0.07-0.15 (0.11)	0.07-0.23 (0.15)
MgO	45.8-50.5 (48.9)	31.5-34.7 (33.2)	14.2-17.7 (15.9)	13.8-22.7 (19.3)	44.1-50.2 (46.7)	31.4-34.1 (32.4)	15.2-16.8 (16.0)	12.2-18.4 (16.1)	37.1-49.2 (44.0)	–	13.6-17.4 (14.9)	14.4-22.9 (17.5)
CaO	0.04-0.16 (0.08)	0.50-0.99 (0.74)	18.0-23.2 (21.2)	–	0.08-0.20 (0.13)	0.63-1.52 (1.09)	20.1-21.8 (20.6)	–	0.03-0.24 (0.12)	–	17.2-22.5 (21.0)	–
Na_2O	–	0.004-0.16 (0.07)	0.25-2.06 (1.19)	–	–	0.07-0.14 (0.08)	0.82-1.55 (1.09)	–	–	–	0.31-1.54 (0.90)	–
NiO	0.27-0.42 (0.37)	–	–	0.16-0.43 (0.32)	0.22-0.35 (0.31)	–	–	0.13-0.32 (0.25)	0.07-0.42 (0.22)	–	–	0.09-0.29 (0.17)
Mg#	0.86-0.91 (0.90)	0.88-0.92 (0.90)	0.88-0.95 (0.91)	0.64-0.88 (0.78)	0.83-0.90 (0.86)	0.86-0.91 (0.88)	0.85-0.91 (0.88)	0.56-0.75 (0.67)	0.72-0.90 (0.83)	–	0.79-0.93 (0.86)	0.61-0.88 (0.70)
Cr#	–	–	–	0.02-0.64 (0.22)	–	–	–	0.13-0.54 (0.29)	–	–	–	0.002-0.42 (0.13)

composition ratios (<1) (*Figure 3*; *Supplementary Table 1*). Olivine, orthopyroxene and clinopyroxene have higher average Mg-numbers in Supergroup I/a (0.90, 0.90, 0.91, respectively) compared to the Supergroup I/b xenoliths (0.86, 0.88, 0.88, respectively) (*Figure 4, a, b, d, e*; *Table I*).

The investigated NGVF xenoliths were classified into 17 groups based on the cluster analysis (*Figure 5; Supplementary Table 1*). Supergroup I/a contains the Groups 1–9 (*Figure 5*) with altogether 82 xenoliths (*Supplementary Table 1*), whereas Supergroup I/b includes Groups 10–13 (*Figure 5*) with 17 xenoliths (*Supplementary Table I*). Supergroup II contains four groups (Group 14–17) with 10 xenoliths and two veins that appear within wall rocks classified into Supergroup I/a (*Figure 5*; *Supplementary Table I*). The most populous group is Group 1 with 58 members. The rest of the groups contain ≤9 xenoliths (*Figure 5*). There is one group (Group 11) with only one member (*Figure 5*).

Group 1 xenoliths are present in all localities except Nagy-Salgó (NNS) and Bárna-Kiskő (NBK), and they are dominant (>50%) in six localities (Podrečany [Patakalja] (NPY); Mašková [Maskófalva] (NMS); Jelšovec [Jelsőc] (NJS); Fil'akovo-Kerčik [Fülek–Kercsik-tető] (NFL); Trebel'ovce [Terbeléd] (NTB); Eresztvény (NME) (*Figure 6*). Among the other groups with more than one member, there are some which appear to be restricted to certain localities, such as Group 3 to Bárna-Nagykő (NBN) or Group 4 to Fil'akovské Kováče [Fülekkovácsi] (NFK) (*Figure 6*). The xenoliths of Group 7, Group 8 and Group 13 were collected in neighboring localities (Fil'akovo-Kerčik [Fülek–Kercsik-tető] (NFL) and Fil'akovské Kováče [Fülekkovácsi] (NFK); Mašková [Maskófalva] (NMS) and Jelšovec [Jelsőc] (NJS); Fil'akovo-Kerčik [Fülek–Kercsik-tető]

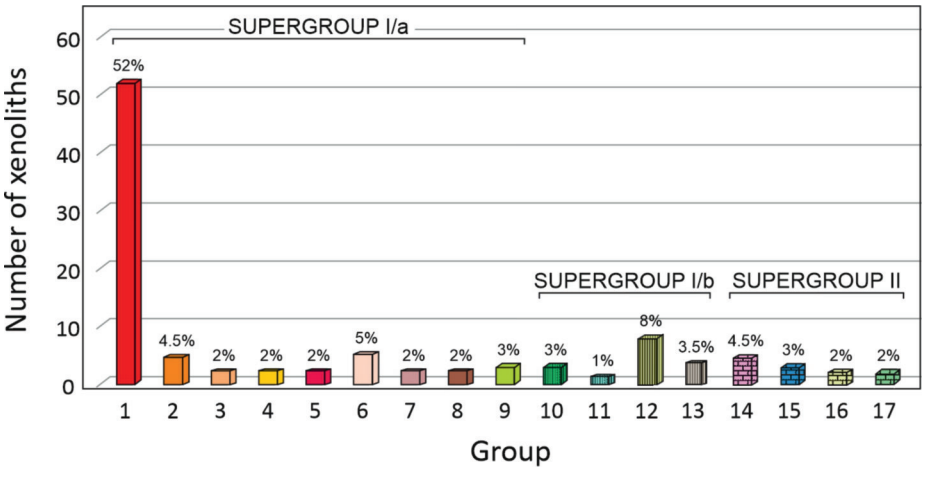

Figure 5. Column chart showing the prevalence of different xenolith groups. The frequency of each group is given in percentage on the top of all columns. Note that one of the xenoliths of the two-membered Group 13 belong to Supergroup I/a and the other to Supergroup I/b

5. ábra. *A xenolitcsoportok gyakoriságát bemutató oszlopdiagram. A csoportok gyakoriságának százalékban kifejezett értéke leolvasható az oszlopok tetején. A két xenolitot magába foglaló 13-as csoport egyik tagja az I/a míg a másik az I/b szupercsoporthoz tartozik*

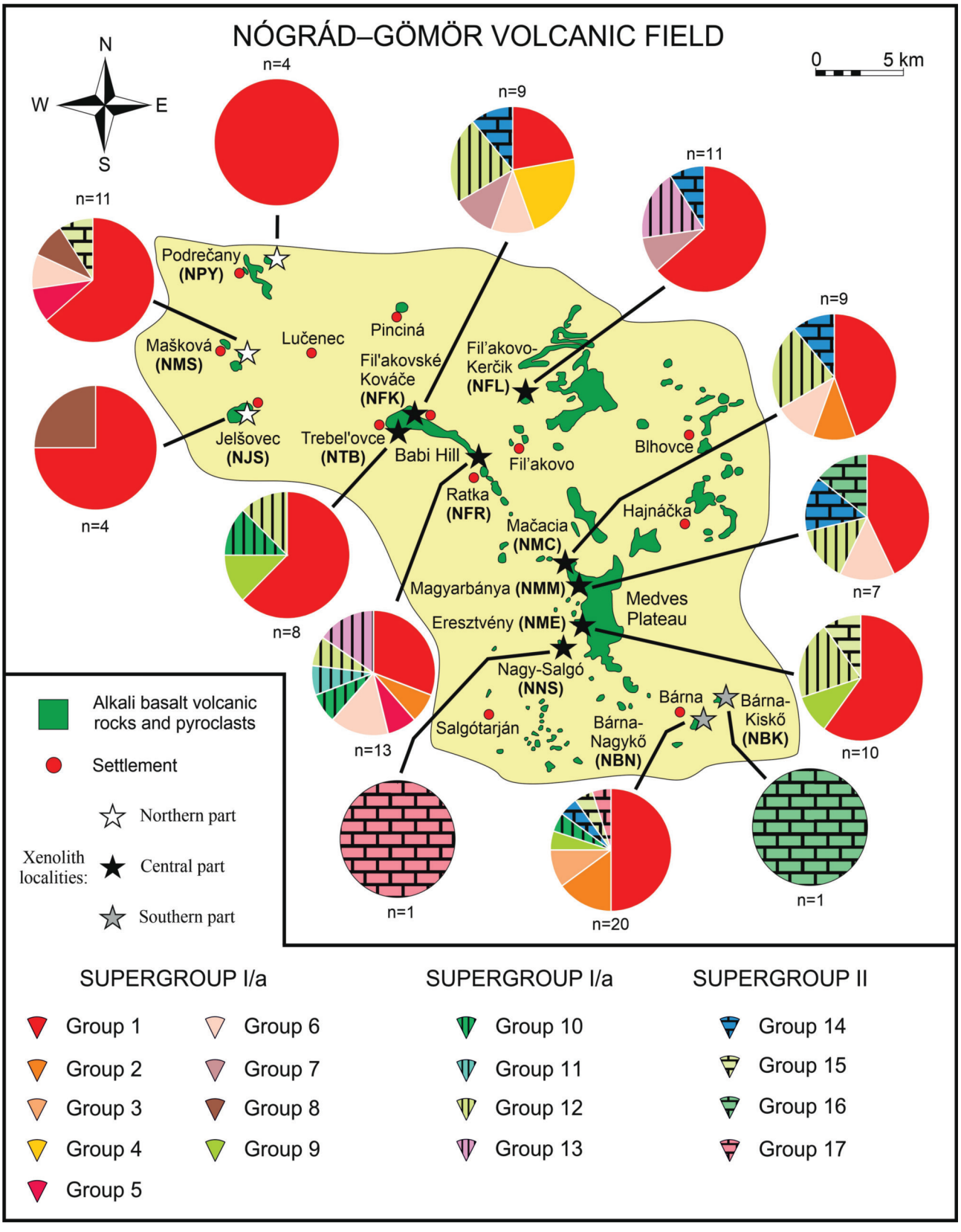

Figure 6. Spatial distribution of xenolith groups in the Nógrád–Gömör Volcanic Field. Alkali basalt outcrops are modified after Jugovics (1971)
6. ábra. *A xenolitcsoportok területi eloszlása a Nógrád–Gömör Vulkáni Területen. Alkáli bazalt előfordulások Jugovics (1971) után módosítva*

(NFL) and Ratka [Rátka] (NFR), respectively) (*Figure 6*). The occurrence of more than 80% of Supergroup I/b and Supergroup II xenoliths is limited to the central part of the NGVF (*Figure 6*).

Group 1 xenoliths dominantly have lherzolitic modal composition with only one dunite xenolith (*Figure 3, a*). It is only Group 3 and Group 7 within Supergroup I/a, where other peridotitic lithologies, dunite and harzburgite also appear (*Supplementary Table I*). Besides the peridotites, one pyroxenite xenolith, namely an olivine websterite, was also classified with the Supergroup I/a xenoliths, constituting a two-membered group (Group 8) (*Figure 3, b*). Among the 17 xenoliths representing Supergroup I/b, only four have lherzolitic modal composition (*Figure 3, c*). Two out of these lherzolites have equal or higher clinopyroxene content over the orthopyroxenes (*Supplementary Table I*). Similarly, xenoliths that belong to Supergroup II are rich in clinopyroxene (>12 vol.%), but completely lack orthopyroxenes and have variable olivine contents (3–85 vol.%) leading to wehrlite, olivine-clinopyroxenite and clinopyroxenite lithologies (*Figure 3, d*; *Table I*).

There are significant differences among the supergroups with respect to the major elements of the rock-forming minerals (*Figure 4*; *Table I*). Supergroup I/a xenoliths have higher Mg# (0.86–0.91 with both an average and median of 0.90) and NiO (0.27–0.42 with an average of 0.37 wt.%) contents in olivine compared to those for Supergroup I/b (0.83–0.90 with an average and median of 0.86 and 0.22–0.35 with an average of 0.31 wt.%, respectively) and Supergroup II (0.72–0.90 with an average and median of 0.83 and 0.84, respectively, and 0.07–0.42 with an average of 0.22 wt.%, respectively) xenoliths (*Figure 4, a*; *Table I*). The ranges of Mg# and MnO in orthopyroxenes for Supergroup I/a (0.88–0.92 with an average of 0.90 and 0.08–0.23 with an average of 0.15 wt.%, respectively) and Supergroup I/b (0.86–0.91 with an average of 0.88 and 0.14–0.29 with an average of 0.21 wt.%, respectively) are overlapping well with only slight differences for average values (*Figure 4, b*; *Table I*). The Al_2O_3 content in clinopyroxenes is somewhat higher in Supergroup II (2.39–9.09 with an average and median of 5.88 and 5.76 wt.%, respectively) with respect to the xenoliths of Supergroup I/a (2.02–7.64 with an average of 5.26 wt.%) or Supergroup I/b (3.39–6.15 with an average of 4.88 wt.%) (*Figure 4, c*; *Table I*). In contrast, the xenoliths of Supergroup I/b have unequivocally lower Mg# (0.85–0.91 with an average of 0.88) and SiO_2 (50.5–53.2 with an average of 51.6 wt.%) and higher TiO_2 (0.19–0.96 with an average of 0.48 wt.%) content in clinopyroxenes compared to the Supergroup I/a xenoliths (0.88–0.95 with an average of 0.91; 50.6–56.2 with an average of 52.1 wt.% and 0.05–1.16 with an average of 0.35 wt.%, respectively). Supergroup II xenoliths show even lower clinopyroxene Mg# (0.79–0.93 with an average of 0.86) and SiO_2 (47.1–54.3 with an average of 50.5 wt.%) concentrations and the highest TiO_2 (0.14–1.97 with an average of 0.86 wt.%) data (*Figure 4, d-e*; *Table I*). In spinels, Supergroups I/b-II have higher TiO_2 contents (0.32–1.08 with an average of 0.61 wt.% and 0.14–0.93 with an average of 0.56 wt.%) compared to Supergroup I/a (0.03–0.49 with an average of 0.14 wt.%) depicted on the Al_2O_3-Cr_2O_3-TiO_2*100 triangle (*Figure 4, f*; *Table I*).

Discussion

Ambient mantle characteristics – significance of Group 1 xenoliths (Supergroup I)

The cluster analysis revealed that Group 1 contains a markedly larger number of samples than any other identified groups (*Figure 5*). This group includes 58 xenoliths which make up 52% of all successfully classified xenoliths. This type of xenoliths occur in all localities with the exception of Nagy-Salgó (NNS) and Bárna-Kiskő (NBK) (*Figure 6*). These observations suggest that Group I xenoliths can be interpreted as the background or ambient mantle in the NGVF (*Table 2*) that was geochemically modified along melt and fluid migration paths leading to rocks of other groups.

Among the 11 localities where Group 1 xenoliths are present, in six outcrops, namely in Podrečany [Patakalja] (NPY), Mašková [Maskófalva] NMS, Jelšovec [Jelsőc] (NJS), Fil'akovo-Kerčik [Fülek–Kercsik-tető] (NFL), Trebel'ovce [Terbeléd] (NTB) and Eresztvény (NME) more than half of the studied xenoliths belong to the Group 1 (*Figure 6*). In the NPY locality, exclusively Group 1 xenoliths were found (*Figure 6*). Three (NPY, NMS, NJS) out of these six localities are situated in the northern part of the NGVF (*Figure 1, b*). These localities represent the oldest volcanic phase in the NGVF that occurred 7–5.9 Ma ago (HURAI et al. 2013). This first volcanic phase was followed by five further phases (HURAI et al. 2013). The youngest volcanic edifices on the surface have ages of <1 Ma (HURAI et al. 2013). The discovery of a low electrical resistivity (<1 m) volume underneath the Moho in the central-NGVF using long period magnetotelluric (MT) measurements and subsequent numerical modelling concluded that small amount (2–3 vol.%) of interconnected melt may occur in the lithospheric mantle of the NGVF even today (PATKÓ et al. 2021a). Note that similar low electrical resistivity (<10 m) volumes were recently discovered underneath the Moho in the rootzones of young (Pleistocene–Holocene) monogenetic volcanic fields in northeast China (ZHAO et al. 2022, DONG et al. 2023, LI et al. 2024) and West Bohemia (PLATZ et al. 2022).

All these suggest that intensive migration of melts and fluids took place in the upper mantle beneath the NGVF during the last 7 Ma and this process is likely still happening now, resulting in various metasomatic alterations at subcrustal depths. The effect of these metasomatic reactions is likely less pronounced in xenoliths that were transported to the surface during the first (oldest) volcanic phase. In contrast, mantle xenoliths that had been entrained into younger host basalts were likely subjected to more fluid and melt fluxes linked to the long-lasting alkali basaltic volcanism. Indeed, Group 1 xenoliths are less-frequently the dominant rocks within the central and southern segments of the NGVF (in 3 out of 10 localities) (*Figure 6*) which formed during younger volcanic phases (<3 Ma). This suggests that the ambient mantle represented by the Group 1 xenoliths (*Table II*) most likely represent mantle segments formed before the

Table II. Estimated modal and geochemical composition of the background (ambient) mantle underneath the NGVF using the average values of the Group 1 xenoliths. Bulk rock data were determined based on mass balance calculations using the average modal and mineral compositions

Abbreviations: ol – olivine; opx – orthopyroxene; cpx – clinopyroxene; sp – spinel

II. táblázat. *A Nógrád-Gömör Vulkáni Terület alatti átlagos (háttér) felsőköpeny becsült ásványos és geokémiai összetétele az 1-es csoportba tartozó xenolitok alapján. A teljeskőzet (bulk rock) adatok az átlagos ásványos összetételek és ásvány-geokémiai adatok felhasználása mellett, tömegegyensúly-számítással készültek*

Rövidítések: ol – olivin; opx – ortopiroxén; cpx – klinopiroxén; sp – spinell

	ol	opx	cpx	sp	bulk
modal composition	72	17	9	2	–
SiO_2	40.8	55.4	52.0	–	43.5
TiO_2	–	0.08	0.36	0.13	0.05
Al_2O_3	–	3.77	5.42	48.5	2.10
Cr_2O_3	–	0.44	0.97	18.8	0.54
FeO	9.78	6.27	2.78	12.4	8.60
MnO	0.14	0.14	0.08	0.12	0.14
MgO	49.1	33.2	15.9	19.4	42.8
CaO	0.07	0.75	21.1	–	2.08
Na_2O	–	0.08	1.26	–	0.13
NiO	0.39	–	–	0.32	0.28
Mg#	0.90	0.91	0.91	0.78	–
Cr#	–	–	–	0.21	–

initiation of the alkali basaltic volcanism. After asthenospheric melts reached shallower depths, the lithospheric mantle was intensely modified especially along melt and fluid migration paths leading to rocks classified into other groups.

Group 1 xenoliths are dominantly lherzolites with only one exception (NBN23 dunite xenolith). Most of the samples correspond to the modal composition of the average European subcontinental lithospheric mantle (SCLM; Downes 1997) using the classification of Streckeisen (1976) (*Figure 3, a*). Only 15 out of the 58 Group 1 xenoliths contain amphibole with a maximum of 3 vol.% modal content, suggesting that modal metasomatism is not a general event affecting these xenoliths. The major element composition of the olivines in Group 1 xenoliths is within a narrow range. The Mg# [Mg#=Mg/(Mg/Fe^{2+})] of olivines varies between 0.88–0.91 (with an average of 0.90) (*Figure 4, a*) agreeing with the average value characteristic for Phanerozoic lithospheric mantle (~0.90; Gaul et al. 2000). Similarly, the orthopyroxenes and clinopyroxenes show uniform geochemistry (Mg# range is between, 0.88–0.92 and 0.89–0.94, respectively) (*Figure 4, b* and *d*). Note that data on 38 out of 58 Group 1 xenoliths were published by Liptai et al. (2017), who classified the 51 xenoliths they studied into four groups (IA, IB, IIA, IIB) based on the major- and trace element characteristics of their rock-forming minerals. In order to clearly distinguish the groups defined by Liptai et al. (2017) from the groups established in this study, we use the following terms for prior groups hereafter: LIP-IA, LIP-IB, LIP-IIA, LIP-IIB. Group LIP-I and LIP-II xenoliths have olivine Mg# of 0.89–0.91 and <0.89, respectively. Further division is based on the LREE enrichment (LIP-B subgroup) or depletion (LIP-A subgroup) in pyroxenes. Although trace elements were not considered in the current study, the results revealed that the Group 1 xenoliths dominantly belong to the LIP-IA (14 xenoliths) and LIP-IB (18 xenoliths) groups following the classification of Liptai et al. (2017) (*Supplementary Table I*). In contrast, Group LIP-IIA and LIP-IIB xenoliths are subordinate (NPY1310, NPY1311, NJS1302, NJS1304 and NMC1309, NMM0318 xenoliths, respectively) among the Group 1 xenoliths (*Supplementary Table I*). Liptai et al. (2017) proposed that the Group LIP-IA xenoliths represent mantle segments affected by a minimum of ~7–10% melt extraction. Since Group IA xenoliths, apart from two amphibole-bearing xenoliths (NMS1308; NFL1329), show no evidence of metasomatism (e.g., presence of hydrous phases such as amphibole, LREE enrichment) overprinting the depleted character, Liptai et al. (2017) considered these xenoliths as having formed during the oldest episodes in the NGVF evolution history. In contrast, LIP-IB xenoliths were affected by metasomatism linking to the migration of a mafic melt within intraplate settings (Liptai et al. 2017). This metasomatism left the major element composition of the rocks unchanged, which is the basis of our cluster analysis, and only led to U-Th-Nb-Ta-LREE enrichment in clinopyroxenes (Liptai et al. 2017). This explains why many of the Group LIP-IA and LIP-IB xenoliths were classified into the same group using the CluStress algorithm despite their different proposed origin. The six Group 1 xenoliths classified to the LIP-IIA and LIP-IIB xenolith groups by Liptai et al. (2017) have olivine Mg# values (0.88; *Supplementary Table I*) close to the arbitrarily chosen value of 0.89 distinguishing Group LIP-I and LIP-II.

Depletion and enrichment events in the mantle of the NGVF

Evolution of Group 2-9 xenoliths (Supergroup I/a)

The total number of xenoliths in Groups 2–9 (24 xenoliths) is much lower compared to the number of xenoliths belonging to Group 1 (58 xenoliths) (*Figure 5; Supplementary Table I*). The groups within Supergroup I/a, with the exception of Group 1, contain small numbers of xenoliths (maximum of six; Group 6; *Figure 5*). Note that among the 9 groups belonging to Supergroup I/a, six groups have 3 or fewer members (*Figure 5*).

The low number of the xenoliths within these groups made it challenging to constrain their evolution history properly. Nevertheless, there are several groups where all group member xenoliths were also classified into the same group by Liptai et al. (2017). This suggests a similar origin to all group members, also extending this assumption to xenoliths discussed in other studies such as Hovorka & Fejdi (1980), Szabó & Taylor (1994), Konečný P. et al. (1995), Konečný et al. (1999), Aradi et al. (2013), often resorting to a scant number of analyzed elements (especially trace elements), because of the less advanced instruments available at the time.

Group 2 contains only amphibole-free LIP-IA xenoliths, proposed to have been affected exclusively by depletion,

which was not followed by any episodes of enrichment (LIPTAI et al. 2017). Similarly, the Group LIP-IIA xenoliths that correspond to Groups 1 and 8 dominantly have a protogranular texture (*Supplementary Table I*). They were subjected only to low degree (<5%) melt extraction, meaning that these xenoliths represent the most fertile upper mantle domain in the NGVF (LIPTAI et al. 2017). Such xenoliths with protogranular texture and fertile composition were also found in the Bakony–Balaton Highland Volcanic Field (BBHVF) and were interpreted as prior asthenospheric domains newly accreted to the lithosphere after tectonic inversion (KOVÁCS et al. 2012, PATKÓ et al. 2024). These BBHVF xenoliths had higher equilibrium temperatures, which may indicate a deeper origin. If we compare the results of the rare earth element-based thermometer (T_{REE}; LIANG et al. 2013) for the LIP-IIA and the other xenoliths from the northern segment of the NGVF, we get higher values in the former (1052–1145 with an average of 1076 °C) than in the latter (980–1097 with an average of 1030 °C) xenoliths (LIPTAI et al. 2017). This difference is notable even when we consider the uncertainties of the T_{REE} thermometer. These data suggest that the LIP-IIA xenoliths may also represent a greater depth of the lithospheric mantle compared to the LIP-IA and LIP-IB xenoliths of the northern segment of the NGVF. The T_{REE} data are >100 °C higher than T_{BK} (two pyroxene thermometer of BREY & KÖHLER (1990)) of the same xenoliths, which suggests a recent cooling event in the lithospheric mantle (WANG et al. 2015). The reason for this may be the tectonic inversion and gradual deepening of the lithosphere-asthenosphere boundary in the Pannonian Basin (HORVÁTH & CLOETINGH 1996, BADA et al. 2007).

Group 7 consists partly of the only LIP-IB xenolith (NFL1315A) not classified into the Group 1 (*Supplementary Table I)*. LIP-IB xenoliths were affected by mafic melt metasomatism within intraplate settings leading to U-Th-Nb-Ta-LREE enrichment in clinopyroxenes according to LIPTAI et al. (2017). The reason why xenolith NFL1315A was not classified into Group 1 is probably its harzburgitic modal composition and thus different major element geochemistry such as its slightly lower Al and Ti content for rock-forming minerals compared to those in Group 1 xenoliths (*Supplementary Table I*).

Members of Groups 6 and 9 consist only of xenoliths that were classified into the LIP-IIB (*Supplementary Table I)*. LIPTAI et al. (2017) suggested that these LIP-IIB xenoliths were formed recently, linking to subcrustal melt migration of the Neogene alkali basalt volcanism. Such silica undersaturated melts interact with peridotite wall rock, which can lead to the formation of clinopyroxenes at the expense of orthopyroxenes resulting in clinopyroxene-rich lithologies (MITCHELL & GROVE 2016). Indeed, the LIP-IIB xenolith of Group 6 xenoliths has an orthopyroxene/clinopyroxene ratio <1 (*Supplementary Table I)*. The role of basaltic melt in the formation of Groups 6 and 9 xenoliths are further proved by their so-called basaltic element (Fe, Mn, Ti)-rich character compared to other xenoliths belonging to Supergroup I/a (*Figure 4*).

There is one group (Group 7), where the members include both LIP-IB and LIP-IIB xenoliths (*Supplementary Table 1)*. Note, however, that the evolutionary history of both the LIP-IB and LIP-IIB xenolith groups is related to migrating mafic melts, which makes their major element geochemistry similar to each other (LIPTAI et al. 2017).

The reason why xenoliths formed in a single event were often classified into more groups is possibly due to minor geochemical differences in the products reflecting distinct starting materials, different degree of metasomatism / partial melting, metasomatic agent changes along migration channels, etc.

Wehrlitization – formation of Group 10–13 xenoliths (Supergroup I/b)

Supergroup I/b dominantly has wehrlite xenolith members classified into four groups (Group 10, 11, 12, 13) (*Figure 5*; *Supplementary Table I)*. In addition to the wehrlites, four lherzolites were also classified into Supergroup I/b. Two out of these four lherzolites have an orthopyroxene/clinopyroxene ratio ≤1 (*Supplementary Table I).* The xenoliths classified into Supergroup I/b, except for one xenolith (NBN0311) originate from southern Bárna-Nagykő (NBN), and were all collected in the central part of the NGVF (*Figure 6*). Twelve wehrlite xenoliths were investigated by PATKÓ et al. (2020) in detail. PATKÓ et al. (2020) defined these rocks as iron-wehrlites, which are known in various tectonic settings all over the world and suggested to have formed as a result of intensive melt-rock reactions between peridotitic wall rocks and silica-undersaturated basaltic melts (PESLIER et al. 2002, IONOV et al. 2005, XIAO et al. 2010, SHAW et al. 2018, LIN et al. 2020). The NGVF wehrlites can be considered as extreme products of the metasomatic event that also led to the formation of LIP-IIB xenoliths, which are dominantly clinopyroxene-rich (clinopyroxene>orthopyroxene) lherzolites. The reason why in some xenoliths almost all orthopyroxene was consumed, whereas in others, the orthopyroxene remained in a high modal presence (sometimes >10 vol.%) can be due to the various melt-rock ratios during the interactions (PATKÓ et al. 2020). The melt-rock ratio is determined by the distance from melt migration channels, meaning that the LIP-IIB lherzolites and wehrlites were likely formed farther away and closer to them, respectively. PATKÓ et al. (2020) suggested that the clinopyroxene-enrichment is associated with a recent melt generation and migration process, which is linked to the same magmatic event as the host basalt volcanism in the Neogene.

The reason why the CluStress algorithm distinguished four groups within Supergroup II can be the different degrees of metasomatism in case of the wehrlites. Note that PATKÓ et al. (2020) classified the wehrlites into three groups, namely highly, moderately and weakly metasomatized xenoliths, referring to the degree of metasomatism constrained mostly by the major element characteristics of the rock-forming minerals. Wehrlite xenoliths in Group 10 are weakly metasomatized (PATKÓ et al. 2020). This weakly-

metasomatized character is further supported by the third member of Group 10, which has a lherzolitic composition (*Supplementary Table I*). Similarly, half of the Group 13 xenoliths are lherzolitic suggesting only a weak metasomatic effect on them (*Supplementary Table I)*. The most populous Group 12 contains highly, moderately and weakly metasomatized wehrlites equally. This suggests that the degree of metasomatism alone is not enough to explain the existence of the four groups within Supergroup I/b. The major element composition of the subordinate orthopyroxenes can be the major factor in distinguishing these groups. Orthopyroxenes in the Group 10, 11 and 13 have narrow compositional ranges, which clearly differs from that of the Group 12 xenoliths (*Figure 4, b*).

Underplating near the Moho – formation of Group 14–17 xenoliths (Supergroup II)

There are four groups (Group 14, 15, 16, 17) that belong to Supergroup II (*Figures 2, 5*). Group 14 consist of five xenoliths including three wehrlites (*Supplementary Table I*). These wehrlites resemble the Supergroup I/b xenoliths regarding their modal composition (*Figure 3, d*) and geochemical characteristics (*Figure 4*). The reason why the cluster analyses sorted these wehrlites in Supergroup II can be the missing orthopyroxenes in them. Note that the lack of orthopyroxenes is a common feature in all Supergroup II xenoliths (*Supplementary Table I*).

The other three groups (Group 15, 16, 17) are all composed of cumulate xenoliths with olivine clinopyroxenite, clinopyroxenite and wehrlite modal compositions (*Figure 3, d*). According to Huraiová et al. (1996), Kovács et al. (2004) and Zajacz et al. (2007), the cumulates are crystallized from basaltic melts near the Moho, resulting in underplated bodies. The cumulate formation, similar to the LIP-IIB and Supergroup I/b xenoliths, is likely related to the alkali basaltic volcanism of the Neogene volcanic activity (Kovács et al. 2004). Magmatic underplating is a well-known process dominantly related to the stagnation of asthenosphere-derived melts in the vicinity of the Moho, leading to local thickening of the crust (Gahlan et al. 2012, Perinelli et al. 2017).

Implications of alkali basalt volcanism in lithospheric mantle evolution underneath the NGVF

According to our results and the outcomes of prior studies (Kovács et al. 2004, Liptai et al. 2017, Patkó et al. 2020), the Neogene alkali basalt volcanism significantly altered the lithospheric mantle underneath the NGVF by forming various new domains (*Figure 7*). Some of these domains were located farther away from melt migration paths and thus were buffered by the pre-Neogene mantle characteristics from petrographic and geochemical points of view. These rocks were classified into Groups 6 and 9 and also appear in Group 7 (*Supplementary Table I*), and were defined as LIP-IIB by Liptai et al. (2017) (*Figure 7*). In areas where the

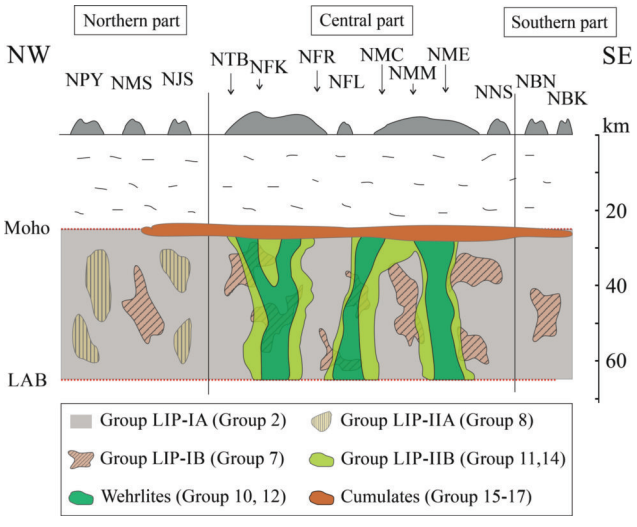

Figure 7. Schematic illustration of the supposed upper mantle domains underneath the NGVF (modified after Liptai et al. 2017). Group numbers in brackets refer to the results of the current study, which can unambiguously link to mantle volumes defined by prior studies (Liptai et al. 2017: LIP-IA, LIP-IIA, LIP-IB, LIP-IIB; Patkó et al. 2020: wehrlite and Kovács et al. 2004: cumulate xenoliths). Depth of Moho and LAB (lithosphere–asthenosphere boundary) in the NGVF are taken from Klébesz et al. (2015). (For abbreviations of the sampling sites see Figure 1, b)

*7. **ábra.** A Nógrád–Gömör Vulkáni Terület alatti felsőköpeny feltételezett egységeit bemutató sematikus ábra (Liptai et al. 2017 alapján). A zárójelben megjelenő csoportok a jelen tanulmányban kerültek meghatározásra és egyértelműen kötődnek korábban definiált köpenytérfogatokhoz (Liptai et al. 2017: LIP-IA, LIP-IIA, LIP-IB, LIP-IIB; Patkó et al. 2020: wehrlit [wehrlite] és Kovács et al. 2004: kumulátum [cumulate] xenolitok). A Klébesz et al. (2015) által meghatározott Moho és litoszféra-asztenoszféra határ (LAB) mélységek Nógrád–Gömörre vonatkoznak. (A xenolit-előfordulások rövidítései megtalálhatók az 1b ábra aláírásában)*

melt-rock ratio was higher (i.e. closer to melt migration channels) wehrlite bodies were formed (Groups 10–13). The appearance of wehrlite xenoliths being largely restricted to the central-NGVF (*Figures 6, 7*) is probably due to tectonic reasons as proposed by Patkó et al. (2021a). The xenoliths included in Group 14, although being sorted in another supergroup (Supergroup II instead of Supergroup I/a), are similar to those appearing in Groups 10–13 (*Supplementary Table I*). The reaction textures (irregular-shaped orthopyroxenes in the core of newly formed clinopyroxenes; figure 2g in Patkó et al. 2020) and the geochemical heterogeneities present even within grains suggest that wehrlite xenoliths are in disequilibrium. These observations further support that these rocks were formed shortly before their entrapment into the host basalt. The upward migrating melts may stagnate and crystallize to form cumulates (Groups 14–17) in the vicinity of the Moho (*Figure 7*), the most pronounced discontinuity in the lithosphere. All these reveal that at least 11 groups out of the distinguished 17 (i.e. ~35% of the classified xenoliths) are strongly related to the alkali basaltic volcanism.

In case of xenoliths that were unaffected by the Neogene alkali basaltic melts, further events, including both depletion and enrichment associated with partial melting and metasomatism, respectively, were explored (Liptai et al. 2017) (*Figure 7*). However, these xenoliths (e.g., members of Group 1, 2, 3, 4, 5, 8) show only moderate variation

considering their major element characteristics (*Figure 4*) suggesting that a large proportion of the upper mantle was in chemical equilibrium before the introduction of the first basaltic magma batches in the Neogene. Based on these findings, we assume that in the rootzones of other volcanic fields of the CPR, where intensive basaltic melt migration occurred (HARANGI et al. 2015) in the last ~10 million years (PÉCSKAY et al. 2006), the pre-Neogene petrographic and geochemical characteristics of the lithospheric mantle were overprinted significantly.

Conclusion

1) In this study a database was compiled using the data of 112 upper mantle xenoliths (114 lithologies due to composite samples) from the Nógrád–Gömör Volcanic Field. The database is composed of the major element compositions of the rock-forming minerals (olivine, pyroxenes and spinel). Subsequently, a cluster analysis was implemented on these data leading to the discrimination of three supergroups (I/a, I/b and II) and 17 groups within them.

2) Most of the xenoliths (~50% of all classified xenoliths) were sorted into Group 1 and appear in almost all xenolith-bearing localities in Nógrád–Gömör. The Group 1 xenoliths exhibit narrow compositional ranges with an olivine Mg# of ~0.90. These rocks were considered to represent an ambient lithospheric mantle underneath the study area based on their frequency and spatial distribution.

3) Most of the resulting groups are possibly linked to different events described by former scientific works. For example, Group 2 only includes xenoliths that were affected by variable melt extraction (~5–25%). In contrast, members of Group 10–13 are products of intensive melt-rock reactions, whereas Group 14–17 xenoliths are cumulates formed by basaltic melt crystallization in the vicinity of the Moho.

4) At least 11 groups out of the distinguished 17 (i.e. ~35% of the classified xenoliths) are strongly related to the Neogene alkali basaltic volcanism. This suggests that the pre-Neogene rootzones of volcanic fields in the Carpathian–Pannonian region were significantly modified due to intensive melt-rock reactions between upward migrating basaltic melts and wall rocks taking place in the last ~10 million years.

Acknowledgement

We dedicate this article to Csaba SZABÓ who taught all of us at the Eötvös Loránd University for various courses in the field of earth sciences. Furthermore, Csaba SZABÓ was the supervisor of the Ph.D. research of Nóra LIPTAI and Levente PATKÓ that were carried out in the Lithosphere Fluid Research Lab (LRG) founded by him. The vast knowledge we all gained during these years established our professional lives, thus we express our gratitude to Csaba SZABÓ.

Csaba SZABÓ played a key role in revealing several aspects of the evolution of the lithospheric mantle in the Carpathian–Pannonian region and beyond. The reason why we chose Nógrád–Gömör Volcanic Field as the subject of this case study was primarily because Csaba SZABÓ published several important, xenolith-based scientific papers as a first author from this locality.

We thank the editor Orsolya SZTANÓ and reviewers Enikő BALI and Attila VIRÁG for their constructive comments on an original version of the manuscript, which substantially contributed to improve our work. This research was financially supported by the National Research, Development and Innovation Fund (grant number: 145853) to LP.

References – Irodalom

ARADI, L. E., HIDAS, K., KOVÁCS, I. J., TOMMASI, A., KLÉBESZ, R., GARRIDO, C. J. & SZABÓ, CS. 2017: Fluid-enhanced annealing in the subcontinental lithospheric mantle beneath the westernmost margin of the Carpathian–Pannonian extensional basin system. – *Tectonics* **36**, 2987–3011. https://doi.org/10.1002/2017TC004702

ARADI, L. E., SZABÓ, CS., GONZÁLEZ-JIMÉNEZ, J. M., GRIFFIN, W., O'REILLY, S. Y. & HATTORI, K. 2013: Ancient fragments in the subcontinental lithospheric mantle beneath the Carpathian-Pannonian region. – *Mineralogical Magazine* **77**, 605.

BADA, G., HORVÁTH, F., DÖVÉNYI, P., SZAFIÁN, P., WINDHOFFER, G. & CLOETINGH, S. 2007: Present-day stress field and tectonic inversion in the Pannonian basin. – *Global and Planetary Change* **58**, 165–180. https://doi.org/10.1016/j.gloplacha.2007.01.007

BALÁZS, A., MAȚENCO, L., MAGYAR, I., HORVÁTH, F. & CLOETINGH, S. A. P. L. 2016: The link between tectonics and sedimentation in back-arc basins: New genetic constraints from the analysis of the Pannonian Basin. – *Tectonics* **35**, 1526–1559. https://doi.org/10.1002/2015TC004109

BALI, E., FALUS, GY., SZABÓ, CS., PEATE, D. W., HIDAS, K., TÖRÖK, K. & NTAFLOS, T. 2007: Remnants of boninitic melts in the upper mantle beneath the central Pannonian Basin? – *Mineralogy and Petrology* **90**, 51–72. https://doi.org/10.1007/s00710-006-0167-z

BALI, E., HIDAS, K., GUÐFINNSSON, G. H., KOVÁCS, Z., TÖRÖK, K. & ROMÁN-ALPISTE, M. J. 2018: Zircon and apatite-bearing pyroxene hornblendite mantle xenolith from Hungary, Carpathian–Pannonian region. – *Lithos* **316**, 19–32. https://doi.org/10.1016/j.lithos.2018.07.004

BALOGH, K., MIHALIKOVÁ, A. & VASS, D. 1981: Radiometric dating of basalts in southern and central Slovakia. – *Západné Karpaty, séria geológia* **7**, 113–126.

BERKESI, M., GUZMICS, T., SZABÓ, CS., DUBESSY, J., BODNAR, R. J., HIDAS, K. & RATTER, K. 2012: The role of CO_2-rich fluids in trace element transport and metasomatism in the lithospheric mantle beneath the Central Pannonian Basin, Hungary, based on fluid inclusions in mantle xenoliths. – *Earth and Planetary Science Letters* **331**, 8–20. https://doi.org/10.1016/j.epsl.2012.03.012

BOROVEC, Z. 1996: Evaluation of the concentrations of trace elements in stream sediments by factor and cluster analysis and the sequential extraction procedure. – *Science of the Total environment* **177**, 237–250. https://doi.org/10.1016/0048-9697(95)04901-0

Boschetty, F. O., Ferguson, D. J., Cortés, J. A., Morgado, E., Ebmeier, S. K., Morgan, D. J., Romero, J. E. & Silva Parejas, C. 2022: Insights into magma storage beneath a frequently erupting arc volcano (Villarrica, Chile) from unsupervised machine learning analysis of mineral compositions. – *Geochemistry, Geophysics, Geosystems* **23**, e2022GC010333. https://doi.org/10.1029/2022GC010333

Box, G. E. & Cox, D. R. 1964: An analysis of transformations. – *Journal of the Royal Statistical Society Series B: Statistical Methodology* **26**, 21–1243. https://doi.org/10.1111/j.2517-6161.1964.tb00553.x

Brey, G. P. & Köhler, T. 1990: Geothermobarometry in four-phase lherzolites II. New thermobarometers, and practical assessment of existing thermobarometers. – *Journal of Petrology* **31**, 1353–1378. https://doi.org/10.1093/petrology/31.6.1353

Campello, R. J. G. B., Moulavi, D. & Sander, J. 2013: Density-Based Clustering Based on Hierarchical Density Estimates. – In: Pei, J. et al. (eds): *Advances in knowledge discovery and data mining*. Springer, 160–172. https://doi.org/10.1007/978-3-642-37456-2_14

Coltorti, M., Bonadiman, C., Faccini, B., Ntaflos, T. & Siena, F. 2007: Slab melt and intraplate metasomatism in Kapfenstein mantle xenoliths (Styrian Basin, Austria). – *Lithos* **94**, 66–89. https://doi.org/10.1016/j.lithos.2006.07.003

Cortés, J. A., Palma, J. L. & Wilson, M. 2007: Deciphering magma mixing: the application of cluster analysis to the mineral chemistry of crystal populations. – *Journal of Volcanology and Geothermal Research* **165**, 163–188. https://doi.org/10.1016/j.jvolgeores.2007.05.018

Csontos, L. & Nagymarosy, A. 1998: The Mid-Hungarian line: a zone of repeated tectonic inversions. – *Tectonophysics* **297/1–4,** 51–71. https://doi.org/10.1016/S0040-1951(98)00163-2

Csontos, L. & Vörös, A. 2003: Mesozoic plate tectonic reconstruction of the Carpathian region. – *Palaeogeography, Palaeoclimatology, Palaeoecology* **210**, 1–56. https://doi.org/10.1016/j.palaeo.2004.02.033

Czirok, L. & Kuslits, L. 2018: Effects of earthquake data clustering on the results of stress inversions. – *Geosciences and Engineering* **6**, 127–141.

Czirok, L., Kuslits, L., Bozsó, I., Radulian, M. & Gribovszki, K. 2022: Cluster analysis for the study of stress patterns in the Vrancea-Zone (SE-Carpathians). – *Pure and Applied Geophysics* **179**, 3693–3712. https://doi.org/10.1007/s00024-022-03159-w

Dawson, J. B. & Stephens, W. E. 1975: Statistical classification of garnets from kimberlite and associated xenoliths. – *Journal of Geology* **83**, 589–607. https://doi.org/10.1086/628143

Dong, Z., Xiao, Q., Deng, Y., Han, B., Tang, J., Wang, L. & Wang, J. 2023: Preliminary magnetotelluric investigation of crustal magma plumbing system beneath the Wulanhada volcanic field, northern China: Implications for the Magma reservoir and pathway. – *Journal of Volcanology and Geothermal Research* **443**, 107938. https://doi.org/10.1016/j.jvolgeores.2023.107938

Downes, H. 1997: Shallow continental lithospheric mantle heterogeneity – petrological constraints. – In: Fuchs, K. (ed.): *Upper mantle heterogeneities from active and passive seismology*. Springer, 295–308. https://doi.org/10.1007/978-94-015-8979-6_29

Embey-Isztin, A. 1978: On the petrology of spinel lherzolite nodules in basaltic rocks from Hungary and Auvergne, France. – *Annales historico-naturales Musei nationalis hungarici* **70**, 27–44.

Embey-Isztin, A., Scharbert, H. G., Dietrich, H. & Poultidis, H. 1989: Petrology and geochemistry of peridotite xenoliths in alkali basalts from the Transdanubian Volcanic Region, West Hungary. – *Journal of Petrology* **30**, 79–105. https://doi.org/10.1093/petrology/30.1.79

Embey-Isztin, A., Downes, H., James, D. E., Upton, B. G. J., Dobosi, G., Ingram, G. A., Harmon, R. S. & Scharbert, H. G. 1993: The petrogenesis of Pliocene alkaline volcanic rocks from the Pannonian Basin, Eastern Central Europe. – *Journal of Petrology* **34**, 317–343. https://doi.org/10.1093/petrology/34.2.317

Ester, M., Kriegel, H. P., Sander, J. & Xu, X. 1996: A density-based algorithm for discovering clusters in large spatial databases with noise. – *KDD-96 Proceedings* **96**, 226–231.

Falus, Gy., Tommasi, A., Ingrin, J. & Szabó, Cs. 2008: Deformation and seismic anisotropy of the lithospheric mantle in the south-eastern Carpathians inferred from the study of mantle xenoliths. – *Earth and Planetary Science Letters*, **272**, 50–64. https://doi.org/10.1016/j.epsl.2008.04.035

Fodor, L., Csontos, L., Bada, G., Györfi, I. & Benkovics, L. 1999: Tertiary tectonic evolution of the Pannonian Basin system and neighbouring orogens: a new synthesis of palaeostress data. – *Geological Society of London, Special Publications* **156**, 295–334. https://doi.org/10.1144/gsl.sp.1999.156.01.15

Frey, F. A. & Prinz, M. 1978: Ultramafic inclusions from San Carlos, Arizona: petrologic and geochemical data bearing on their petrogenesis. – *Earth and Planetary Science Letters* **38**, 129–176. https://doi.org/10.1016/0012-821X(78)90130-9

Gahlan, H. A., Arai, S., Abu El-Ela, F. F. & Tamura, A. 2012: Origin of wehrlite cumulates in the Moho transition zone of the Neoproterozoic Ras Salatit ophiolite, Central Eastern Desert, Egypt: crustal wehrlites with typical mantle characteristics. – *Contributions to Mineralogy and Petrology* **163**, 225–241. https://doi.org/10.1007/s00410-011-0669-5

Gaul, O. F., Griffin, W. L., O'Reilly, S. Y. & Pearson, N. J. 2000: Mapping olivine composition in the lithospheric mantle. – *Earth and Planetary Science Letters* **182**, 223–235. https://doi.org/10.1016/S0012-821X(00)00243-0

Gleeson, M. L., Gibson, S. A. & Stock, M. J. 2021: Upper mantle mush zones beneath low melt flux ocean island volcanoes: insights from Isla Floreana, Galápagos. – *Journal of Petrology* **61**, egaa094. https://doi.org/10.1093/petrology/egaa094

Gonçalves, M. A., da Silva, D. R., Duuring, P., Gonzalez-Alvarez, I. & Ibrahimi, T. 2024: Mineral exploration and regional surface geochemical datasets: An anomaly detection and k-means clustering exercise applied on laterite in Western Australia. – *Journal of Geochemical Exploration* **258**, 107400. https://doi.org/10.1016/j.gexplo.2024.107400

Harangi, Sz., Downes, H., Kósa, L., Szabó, Cs., Thirlwall, M. F., Mason, P. R. D. & Mattey, D. 2001: Almandine garnet in calc-alkaline volcanic rocks of the Northern Pannonian Basin (Eastern–Central Europe): Geochemistry, petrogenesis and geodynamic implications. – *Journal of Petrology* **42**, 1813–1843. https://doi.org/10.1093/petrology/42.10.1813

Harangi, Sz., Jankovics, M. É., Sági, T., Kiss, B., Lukács, R. & Soós, I. 2015: Origin and geodynamic relationships of the Late Miocene to Quaternary alkaline basalt volcanism in the Pannonian basin, eastern–central Europe. – *International Journal of Earth Sciences* **104**, 2007–2032. https://doi.org/10.1007/s00531-014-1105-7

Hencz, M., Biró, T., Németh, K., Porkoláb, K., Kovács, I. J., Spránitz, T., Cloetingh, S., Szabó, Cs. & Berkesi, M. 2023: Tectonically-determined distribution of monogenetic volcanoes in a compressive tectonic regime: An example from the Pannonian

continental back-arc system (Central Europe). – *Journal of Volcanology and Geothermal Research* **444**, 107940. https://doi.org/10.1016/j.jvolgeores.2023.107940

HIDAS, K., GUZMICS, T., SZABÓ, CS., KOVÁCS, I., BODNAR, R. J., ZAJACZ, Z., NÉDLI, ZS., VACCARI, L. & PERUCCHI, A. 2010: Coexisting silicate melt inclusions and H_2O-bearing, CO_2-rich fluid inclusions in mantle peridotite xenoliths from the Carpathian–Pannonian region (central Hungary). – *Chemical Geology* **274**, 1–18. https://doi.org/10.1016/j.chemgeo.2010.03.004

HORVÁTH, F. 1993: Towards a mechanical model for the formation of the Pannonian basin. – *Tectonophysics* **226**, 333–357. https://doi.org/10.1016/0040-1951(93)90126-5

HORVÁTH, F. & CLOETINGH, S. A. P. L. 1996: Stress-induced late-stage subsidence anomalies in the Pannonian basin. – *Tectonophysics* **266**, 287–300. https://doi.org/10.1016/S0040-1951(96)00194-1

HORVÁTH, F., BADA, G., SZAFIÁN, P., TARI, G., ÁDÁM, A. & CLOETINGH, S. 2006: Formation and deformation of the Pannonian Basin: constraints from observational data. – *Geological Society, London, Memoirs* **32**, 191–206. https://doi.org/10.1144/GSL.MEM.2006.032.01.11

HOVORKA, D. & FEJDI, P. 1980: Spinel peridotite xenoliths in the west Carpathian late Cenozoic alkali basalts and their tectonic significance. – *Bulletin Volcanologique* **43**, 95–106. https://doi.org/10.1007/BF02597614

HUISMANS, R. S., PODLADCHIKOV, Y. Y. & CLOETINGH, S. 2001: Dynamic modeling of the transition from passive to active rifting, application to the Pannonian basin. – *Tectonics* **20**, 1021–1039. https://doi.org/10.1029/2001TC900010

HURAI, V., DANIŠÍK, M., HURAIOVÁ, M., PAQUETTE, J. L. & ÁDÁM, A. 2013: Combined U/Pb and (U–Th)/He geochronometry of basalt maars in Western Carpathians: implications for age of intraplate volcanism and origin of zircon metasomatism. – *Contributions to Mineralogy and Petrology* **166**, 1235–1251. https://doi.org/10.1007/s00410-013-0922-1

HURAIOVÁ, M. & KONEČNÝ, P. 1994: Pressure-temperature conditions and oxidation state of the upper mantle in southern Slovakia. – *Acta Geologica Hungarica* **37**, 29–39.

HURAIOVÁ, M., KONEČNÝ, P., KONEČNÝ, V., SIMON, K. & HURAI, V. 1996: Mafic and salic igneous xenoliths in late Tertiary alkaline basalts: fluid inclusion and mineralogical evidence for a deep-crustal magmatic reservoir in the western Carpathians. – *European Journal of Mineralogy* **8**, 901–916.

HURAIOVÁ, M., DUBESSY, J., KONEČNÝ, P., SIMON, K., KRÁL', J., ZIELINSKI, G., LIPKA, J. & HURAI, V. 2005: Glassy orthopyroxene granodiorites of the Pannonian Basin: tracers of ultra-high-temperature deep-crustal anatexis triggered by Tertiary basaltic volcanism. – *Contributions to Mineralogy and Petrology* **148**, 615–633. https://doi.org/10.1007/s00410-004-0625-8

HURAIOVÁ, M., PAQUETTE, J. L., KONEČNÝ, P., GANNOUN, A. M. & HURAI, V. 2017: Geochemistry, mineralogy, and zircon U–Pb–Hf isotopes in peraluminous A-type granite xenoliths in Pliocene–Pleistocene basalts of northern Pannonian Basin (Slovakia). – *Contributions to Mineralogy and Petrology* **172**, 1–20. https://doi.org/10.1007/s00410-017-1379-4

IONOV, D. A., CHANEFO, I. & BODINIER, J. L. 2005: Origin of Fe-rich lherzolites and wehrlites from Tok, SE Siberia by reactive melt percolation in refractory mantle peridotites. – *Contributions to Mineralogy and Petrology* **150**, 335–353. https://doi.org/10.1007/s00410-005-0026-7

JANSSON, N. F., ALLEN, R. L., SKOGSMO, G. & TAVAKOLI, S. 2022: Principal component analysis and K-means clustering as tools during exploration for Zn skarn deposits and industrial carbonates, Sala area, Sweden. – *Journal of Geochemical Exploration* **233**, 106909. https://doi.org/10.1016/j.gexplo.2021.106909

JERRAM, D. A. & CHEADLE, M. J. 2000: On the cluster analysis of grains and crystals in rocks. – *American Mineralogist* **85**, 47–67. https://doi.org/10.2138/am-2000-0107

JUGOVICS, L. 1971: Észak-magyarországi – Salgótarján környéki – bazaltterületek. – In: *Annual Report of the Geological Institute of Hungary*, 145–167.

KALKREUTH, W., HOLZ, M., MEXIAS, A., BALBINOT, M., LEVANDOWSKI, J., WILLETT, J., FINKELMAN, R. & BURGER, H. 2010: Depositional setting, petrology and chemistry of permian coals from the paraná basin: 2. South Santa Catarina coalfield, Brazil. – *International Journal of Coal Geology* **84**, 213–236. https://doi.org/10.1016/j.coal.2010.08.008

KALMÁR, D., PETRESCU, L., STIPČEVIĆ, J., BALÁZS, A., KOVÁCS, I. J. & ALPARRAY and PACASE Working Groups 2023: Lithospheric Structure of the Circum-Pannonian Region Imaged by S-To-P Receiver Functions. – *Geochemistry, Geophysics, Geosystems* **24**, e2023GC010937. https://doi.org/10.1029/2023GC010937

KÁZMÉR, M. & KOVÁCS, S. 1985: Permian–Paleogene paleogeography along the eastern part of the Insubric-Periadriatic lineament system: evidence for continental escape of the Bakony–Drauzug unit. – *Acta Geologica Hungarica* **28**, 71–84.

KIM, W., DOH, S. J., YU, Y. & LEE, Y. I. 2013: Magnetic evaluation of sediment provenance in the northern East China Sea using fuzzy c-means cluster analysis. – *Marine Geology* **337**, 9–19. https://doi.org/10.1016/j.margeo.2013.01.001

KLÉBESZ, R., GRÁCZER, Z., SZANYI, GY., LIPTAI, N., KOVÁCS, I., PATKÓ, L., PINTÉR, ZS., FALUS, GY., WESZTERGOM, V. & SZABÓ, CS. 2015: Constraints on the thickness and seismic properties of the lithosphere in an extensional setting (Nógrád–Gömör Volcanic Field, Northern Pannonian Basin). – *Acta Geodaetica et Geophysica* **50**, 133–149. https://doi.org/10.1007/s40328-014-0094-0

KONEČNÝ, P., KONEČNÝ, V., LEXA, J. & HURAIOVÁ, M. 1995: Mantle xenoliths in alkali basalts of Southern Slovakia. – *Acta Vulcanologica* **7,** 241–248.

KONEČNÝ, P., HURAIOVÁ, M. & BIELIK, M. 1999: P–T–X–O_2 conditions in upper mantle: evidence from lherzolitic xenoliths hosted by Plio-Pleistocene alkali basalts. – *Geolines* **9**, 59–66.

KONEČNÝ, V., LEXA, J., BALOGH, K. & KONEČNÝ, P. 1995: Alkali basalt volcanism in Southern Slovakia: volcanic forms and time evolution. – *Acta Vulcanologica* **7**, 167–172.

KOVÁCS, I. & SZABÓ, CS. 2005: Petrology and geochemistry of granulite xenoliths beneath the Nógrád-Gömör volcanic field, Carpathian-Pannonian region (N-Hungary/S-Slovakia). – *Mineralogy and Petrology* **85**, 269–290. https://doi.org/10.1007/s00710-005-0090-8

KOVÁCS, I. & SZABÓ, CS. 2008: Middle Miocene volcanism in the vicinity of the Middle Hungarian zone: evidence for an inherited enriched mantle source. – *Journal of Geodynamics* **45**, 1–17. https://doi.org/10.1016/j.jog.2007.06.002

KOVÁCS, I., FALUS, GY., STUART, G., HIDAS, K., SZABÓ, CS., FLOWER, M. F. J., HEGEDŰS, E., POSGAY, K. & ZILAHI-SEBESS, L. 2012: Seismic anisotropy and deformation patterns in upper mantle xenoliths from the central Carpathian–Pannonian region: Asthenospheric flow as a driving force for Cenozoic extension and extrusion? – *Tectonophysics*, **514**, 168–179. https://doi.org/10.1016/j.tecto.2011.10.022

Kovács, I., Patkó, L., Liptai, N., Lange, T. P., Taracsák, Z., Cloetingh, S. A. P. L., Török, K., Király, E., Karátson, D., Biró, T., Kiss, J., Pálos, Zs., Aradi, L. E., Falus, Gy., Hidas, K., Berkesi, M., Koptev, A., Novák, A., Wesztergom, V., Fancsik, T. & Szabó, Cs. 2020: The role of water and compression in the genesis of alkaline basalts: Inferences from the Carpathian–Pannonian region. – *Lithos* **354**, 105323. https://doi.org/10.1016/j.lithos.2019.105323

Kovács, I., Zajacz, Z. & Szabó, Cs. 2004: Type-II xenoliths and related metasomatism from the Nógrád-Gömör Volcanic Field, Carpathian–Pannonian region (northern Hungary–southern Slovakia). – *Tectonophysics* **393**, 139–161. https://doi.org/10.1016/j.tecto.2004.07.032

Lach-hab, M., Yang, S., Vaisman, I. I. & Blaisten-Barojas, E. 2010: Novel approach for clustering zeolite crystal structures. – *Molecular Informatics* **29**, 297–301. https://doi.org/10.1002/minf.200900072

Lange, T. P., Pálos, Zs., Pósfai, M., Berkesi, M., Pekker, P., Szabó, Á., Szabó, Cs. & Kovács, I. J. 2023: Nanoscale hydrous silicate melt inclusions at the clinopyroxene-amphibole interface in a mantle xenolith from the Per ani Mountains Volcanic Field. – *Lithos* **454**, 107210. https://doi.org/10.1016/j.lithos.2023.107210

Li, Y., Weng, A., Zhou, Z., Guo, J., Li, S., Ventura, G. & Xu, W. 2024: Crustal root shapes the plumbing system of a monogenetic volcanic field as revealed by magnetotelluric data. – *Earth and Planetary Science Letters* **626**, 118523. https://doi.org/10.1016/j.epsl.2023.118523

Liang, Y., Sun, C. & Yao, L. 2013: A REE-in-two-pyroxene thermometer for mafic and ultramafic rocks. – *Geochimica et Cosmochimica Acta* **102**, 246–260. https://doi.org/10.1016/j.gca.2012.10.035

Lin, A. B., Zheng, J. P., Aulbach, S., Xiong, Q., Pan, S. K. & Gerdes, A. 2020: Causes and consequences of wehrlitization beneath a trans-lithospheric fault: Evidence from Mesozoic basalt–borne wehrlite xenoliths from the Tan-Lu fault belt, North China Craton. – *Journal of Geophysical Research: Solid Earth* **125**, e2019JB019084. https://doi.org/10.1029/2019JB019084

Liptai, N., Patkó, L., Kovács, I. J., Hidas, K., Pintér, Zs., Jeffries, T., Zajacz, Z., O'Reilly, S. Y., Griffin, W. L., Pearson, N. J. & Szabó, Cs. 2017: Multiple metasomatism beneath the Nógrád–Gömör Volcanic Field (Northern Pannonian Basin) revealed by upper mantle peridotite xenoliths. – *Journal of Petrology* **58**, 1107–1144. https://doi.org/10.1093/petrology/egx048

Liptai, N., Hidas, K., Tommasi, A., Patkó, L., Kovács, I. J., Griffin, W. L., O'Reilly, S. Y., Pearson, N. J. & Szabó, Cs. 2019: Lateral and vertical heterogeneity in the lithospheric mantle at the northern margin of the Pannonian Basin reconstructed from peridotite xenolith microstructures. – *Journal of Geophysical Research: Solid Earth* **124**, 6315–6336. https://doi.org/10.1029/2018JB016582

Liptai, N., Berkesi, M., Patkó, L., Bodnar, R. J., O'Reilly, S. Y., Griffin, W. L. & Szabó, Cs. 2021: Characterization of the metasomatizing agent in the upper mantle beneath the northern Pannonian Basin based on Raman imaging, FIB-SEM, and LA-ICP-MS analyses of silicate melt inclusions in spinel peridotite. – *American Mineralogist* **106**, 685–700. https://doi.org/10.2138/am-2021-7292

McInnes, L., Healy, J. & Astels, S. 2017: hdbscan: Hierarchical density based clustering. – *Journal of Open Source Software* **2**, 205. https://doi.org/10.21105/joss.00205

McInnes, L., Healy, J. & Melville, J. 2020. Umap: Uniform manifold approximation and projection for dimension reduction. – *arXiv preprint*, arXiv:1802.03426. https://doi.org/10.48550/arXiv.1912.12180

Mitchell, A. L. & Grove, T. L. 2016: Experiments on melt–rock reaction in the shallow mantle wedge. – *Contributions to Mineralogy and Petrology* **171**, 1–21. https://doi.org/10.1007/s00410-016-1312-2

Murphy, K. P. 2012: Machine learning: a probabilistic perspective. – MIT press. p. 1096.

Patkó, L., Liptai, N., Aradi, L. E., Klébesz, R., Sendula, E., Bodnar, R. J., Kovács, I. J., Hidas, K., Cesare, B., Novák, A., Trásy, B. & Szabó, Cs. 2020: Metasomatism-induced wehrlite formation in the upper mantle beneath the Nógrád–Gömör Volcanic Field (Northern Pannonian Basin): Evidence from xenoliths. – *Geoscience Frontiers* **11**, 943–964. https://doi.org/10.1016/j.gsf.2019.09.012

Patkó, L., Novák, A., Klébesz, R., Liptai, N., Lange, T. P., Molnár, G., Csontos, L., Wesztergom, V., Kovács, I. J. & Szabó, Cs. 2021a: Effect of metasomatism on the electrical resistivity of the lithospheric mantle–An integrated research using magnetotelluric sounding and xenoliths beneath the Nógrád–Gömör Volcanic Field. – *Global and Planetary Change* **197**, 103389. https://doi.org/10.1016/j.gloplacha.2020.103389

Patkó, L., Ciążela, J., Aradi, L. E., Liptai, N., Pieterek, B., Berkesi, M., Lazarov, M., Kovács, I. J., Holtz, F. & Szabó, Cs. 2021b: Iron isotope and trace metal variations during mantle metasomatism: In situ study on sulfide minerals from peridotite xenoliths from Nógrád-Gömör Volcanic Field (Northern Pannonian Basin). – *Lithos* **396**, 106238. https://doi.org/10.1016/j.lithos.2021.106238

Patkó, L., Liptai, N., Aradi, L. E., Török, K., Kovács, Z., Kővágó, Á., Gergely, Sz., Kovács, I. J., Szabó, Cs. & Berkesi, M. 2024: Fossil metasomatized and newly-accreted fertilized lithospheric mantle volumes beneath the Bakony-Balaton Highland Volcanic Field (central Carpathian–Pannonian region) – *Lithos* **482–483**, 107701. https://doi.org/10.1016/j.lithos.2024.107701

Pécskay, Z., Lexa, J., Szakács, A., Seghedi, I., Balogh, K., Konečný V., Zelenka, T. Kovacs, M., Póka, T., Fülöp, A., Márton, E., Panaiotu, C. & Cvetković, V. 2006: Geochronology of Neogene magmatism in the Carpathian arc and intra-Carpathian area. – *Geologica Carpathica* **57**, 511–530.

Pedregosa, F., Varoquaux, G., Gramfort, A., Michel, V., Thirion, B., Grisel, O., Blondel, M., Prettenhofer, P., Weiss, R., Dubourg, V., Vanderplas, J., Passos, A., Cournapeau, D., Brucher, M., Perrot, M. & Duchesnay, É. 2011: Scikit-learn: Machine learning in Python. – *Journal of Machine Learning Research* **12**, 2825–2830.

Perinelli, C., Gaeta, M. & Armienti, P. 2017: Cumulate xenoliths from Mt. Overlord, northern Victoria Land, Antarctica: a window into high pressure storage and differentiation of mantle-derived basalts. – *Lithos* **268**, 225–239. https://doi.org/10.1016/j.lithos.2016.10.027

Peslier, A. H., Francis, D. & Ludden, J. 2002: The lithospheric mantle beneath continental margins: melting and melt–rock reaction in Canadian Cordillera xenoliths. – *Journal of Petrology* **43**, 2013–2047. https://doi.org/10.1093/petrology/43.11.2013

Platz, A., Weckmann, U., Pek, J., Kováčiková, S., Klanica, R., Mair, J. & Aleid, B. 2022: 3D imaging of the subsurface electrical resistivity structure in West Bohemia/Upper Palatinate covering mofettes and Quaternary volcanic structures by using Magneto-tellurics. – *Tectonophysics* **833**, 229353. https://doi.org/10.1016/j.tecto.2022.229353

Royden, L. H., Horváth, F. & Burchfiel, B. C. 1982: Transform faulting, extension, and subduction in the Carpathian Pannonian region. – *Geological Society of America Bulletin* **93**, 717–725. https://doi.org/10.1130/0016-7606(1982)93<717:TFEASI>2.0.CO;2

RUBÓCZKI, T., NOVÁK, A., LIPTAI, N., PORKOLÁB, K., MOLNÁR, CS., GALSA, A., MOLNÁR, G., WESZTERGOM, V. & KOVÁCS, I. J. 2024: The Pannon LitH$_2$Oscope magnetotelluric array in the Pannonian Basin. – *Acta Geodaetica et Geophysica* 1–26. https://doi.org/10.1007/s40328-024-00434-1

SADEGHI, M., CASEY, P., CARRANZA, E. J. M. & LYNCH, E. P. 2024: Principal components analysis and K-means clustering of till geochemical data: Mapping and targeting of prospective areas for lithium exploration in Västernorrland Region, Sweden. – *Ore Geology Reviews* **167**,106002. https://doi.org/10.1016/j.oregeorev.2024.106002

SEGHEDI, I. & DOWNES, H. 2011: Geochemistry and tectonic development of Cenozoic magmatism in the Carpathian–Pannonian region. – *Gondwana Research* **20**, 655–672. https://doi.org/10.1016/j.gr.2011.06.009

SHAW, C. S., LEBERT, B. S. & WOODLAND, A. B. 2018: Thermodynamic modelling of mantle–melt interaction evidenced by veined Wehrlite xenoliths from the Rockeskyllerkopf volcanic complex, west Eifel volcanic field, Germany. – *Journal of Petrology* **59**, 59–86. https://doi.org/10.1093/petrology/egy018

STRECKEISEN, A. 1976: To each plutonic rock its proper name. – *Earth-Science Reviews* **12**, 1–33. https://doi.org/10.1016/0012-8252(76)90052-0

SZABÓ, CS. & BODNAR, R. J. 1995: Chemistry and origin of mantle sulfides in spinel peridotite xenoliths from alkaline basaltic lavas, Nógrád–Gömör Volcanic Field, northern Hungary and southern Slovakia. – *Geochimica et Cosmochimica Acta* **59**, 3917–3927. https://doi.org/10.1016/0016-7037(95)00265-2

SZABÓ, CS. & BODNAR, R. J. 1996: Changing magma ascent rates in the Nograd–Gomor volcanic field northern Hungary southern Slovakia: evidence from CO_2-rich fluid inclusions in metasomatized upper mantle xenoliths. – *Petrology* **4**, 240–249.

SZABÓ, CS. & BODNAR, R. J. 1998: Fluid-inclusion evidence for an upper-mantle origin for green clinopyroxenes in late Cenozoic basanites from the Nógrád–Gömör Volcanic Field, northern Hungary/southern Slovakia. – *International Geology Review* **40**, 765–773. https://doi.org/10.1080/00206819809465237

SZABÓ, CS. & TAYLOR, L. A. 1994: Mantle petrology and geochemistry beneath the Nógrád-Gömör volcanic field, Carpathian–Pannonian region. – *International Geology Review* **36**, 328–358. https://doi.org/10.1080/00206819409465465

SZABÓ, CS., HARANGI, SZ. & CSONTOS, L. 1992: Review of Neogene and Quaternary volcanism of the Carpathian–Pannonian region. – *Tectonophysics* **208**, 243–256. https://doi.org/10.1016/0040-1951(92)90347-9

SZABÓ, CS., BODNAR, R. J. & SOBOLEV, A. V. 1996: Metasomatism associated with subduction-related, volatile-rich silicate melt in the upper mantle beneath the Nógrád–Gömör volcanic field, northern Hungary/southern Slovakia; evidence from silicate melt inclusions. – *European Journal of Mineralogy* **8**, 881–899.

SZABÓ, CS., FALUS, GY., ZAJACZ, Z., KOVÁCS, I. & BALI, E. 2004: Composition and evolution of lithosphere beneath the Carpathian–Pannonian Region: a review. – *Tectonophysics* **393**, 119–137. https://doi.org/10.1016/j.tecto.2004.07.031

VASELLI, O., DOWNES, H., THIRLWALL, M., DOBOSI, G., CORADOSSI, N., SEGHEDI, I., SZAKÁCS, A. & VANNUCCI, R. 1995: Ultramafic xenoliths in Plio-Pleistocene alkali basalts from the Eastern Transylvanian Basin: depleted mantle enriched by vein metasomatism. – *Journal of Petrology* **36**, 23–53. https://doi.org/10.1093/petrology/36.1.23

WANG, C., LIANG, Y. & XU, W. 2015: On the significance of temperatures derived from major element and REE based two-pyroxene thermometers for mantle xenoliths from the North China Craton. – *Lithos* **224**, 101–113. https://doi.org/10.1016/j.lithos.2015.01.022

XIAO, Y., ZHANG, H. F., FAN, W. M., YING, J. F., ZHANG, J., ZHAO, X. M. & SU, B. X. 2010: Evolution of lithospheric mantle beneath the Tan-Lu fault zone, eastern North China Craton: evidence from petrology and geochemistry of peridotite xenoliths. – *Lithos* **117**, 229–246. https://doi.org/10.1016/j.lithos.2010.02.017

ZAJACZ, Z. & SZABÓ, CS. 2003: Origin of sulfide inclusions in cumulate xenoliths from Nógrád–Gömör Volcanic Field, Pannonian Basin (north Hungary/south Slovakia). – *Chemical Geology* **194**, 105–117. https://doi.org/10.1016/S0009-2541(02)00273-5

ZAJACZ, Z., KOVÁCS, I., SZABÓ CS., HALTER, W. & PETTKE, T. 2007: Evolution of mafic alkaline melts crystallized in the uppermost lithospheric mantle: a melt inclusion study of olivine-clinopyroxenite xenoliths, northern Hungary. – *Journal of Petrology* **48**, 853–883. https://doi.org/10.1093/petrology/egm004

ZANETTI, A., VANNUCCI, R., OBERTI, R. & DOBOSI, G. 1995: Trace-element composition and crystal-chemistry of mantle amphiboles from the Carpatho-Pannonian Region. – *Acta Vulcanologica* **7**, 265–276.

ZHAO, L., HU, Y., ZHAN, Y., SUN, X., WANG, Q., ZHU, Y. & CAO, C. 2022: Three-dimensional electrical structure and magma system of the monogenetic Longgang Volcanic Field, Northeast China, inferred from Broadband Magnetotelluric Data. – *Journal of Geophysical Research: Solid Earth* **127**, e2022JB024694. https://doi.org/10.1029/2022JB024694

Kézirat beérkezett: 23/02/2024

Digital supplementary

Supplementary Table I. Petrographic and geochemical data of the NGVF xenoliths involved in this study. The localities can be deduced from the sample names or from the abbreviations provided in brackets following the sample names. For explanation of the abbreviations of the sampling sites, see *Figure 1b*

I. kiegészítő táblázat. A jelen tanulmányban vizsgált nógrád-gömöri xenolitok petrográfiai és geokémiai adatai. A mintalelőhelyek kikövetkeztethetők a mintanevekből, ritkábban a mintanevek mögött zárójelben szerepelnek. A mintagyűjtési helyek rövidítéseinek a magyarázatát az 1. ábra képaláírása rögzíti